NOTE TO USERS

Page(s) not included in the original manuscript are unavailable from the author or university. The manuscript was microfilmed as received

Pages 10, 11, 17, 41-45, 47-54, 56-57, 59-62, 64-66, 68-70, 72, 74-79, 81-83, 87-88, 91-93, 95, 97-98, 101-103, 105-107, 109-110, 113-114, 116-117, 121, 124-125, 129-131, 153, 155-165, 167-205

This reproduction is the best copy available.

UMI®

INWARDS VAPOR DIFFUSION DUE TO HIGH TEMPERATURE GRADIENT IN WALL ASSEMBLIES

Saba Saneinejad

A Thesis

in

the Department

of

Building, Civil, and Environmental Engineering

Presented in Partial Fulfillment of the Requirements

for the Degree of Masters of Applied Science (Building Engineering) at

Concordia University

Montreal, Quebec, Canada

April 2009

© Saba Saneinejad 2009

Library and Archives Canada

Published Heritage Branch

395 Wellington Street
Ottawa ON K1A 0N4
Canada

Bibliothèque et Archives Canada

Direction du Patrimoine de l'édition

395, rue Wellington
Ottawa ON K1A 0N4
Canada

Your file Votre référence
ISBN: 978-0-494-63308-3
Our file Notre référence
ISBN: 978-0-494-63308-3

NOTICE:

The author has granted a non-exclusive license allowing Library and Archives Canada to reproduce, publish, archive, preserve, conserve, communicate to the public by telecommunication or on the Internet, loan, distribute and sell theses worldwide, for commercial or non-commercial purposes, in microform, paper, electronic and/or any other formats.

The author retains copyright ownership and moral rights in this thesis. Neither the thesis nor substantial extracts from it may be printed or otherwise reproduced without the author's permission.

AVIS:

L'auteur a accordé une licence non exclusive permettant à la Bibliothèque et Archives Canada de reproduire, publier, archiver, sauvegarder, conserver, transmettre au public par télécommunication ou par l'Internet, prêter, distribuer et vendre des thèses partout dans le monde, à des fins commerciales ou autres, sur support microforme, papier, électronique et/ou autres formats.

L'auteur conserve la propriété du droit d'auteur et des droits moraux qui protège cette thèse. Ni la thèse ni des extraits substantiels de celle-ci ne doivent être imprimés ou autrement reproduits sans son autorisation.

In compliance with the Canadian Privacy Act some supporting forms may have been removed from this thesis.

While these forms may be included in the document page count, their removal does not represent any loss of content from the thesis.

Conformément à la loi canadienne sur la protection de la vie privée, quelques formulaires secondaires ont été enlevés de cette thèse.

Bien que ces formulaires aient inclus dans la pagination, il n'y aura aucun contenu manquant.

Canada

Abstract

Inwards vapor diffusion due to high temperature gradient in wall assemblies

Saba Saneinejad

Moisture is the main source of deterioration of building envelope systems. One source of moisture that has not been studied to a great extent is inwards vapor flows, due to high temperature gradients. Such flows occur, for example, when exterior claddings like brick are wetted by rain and then exposed to solar radiation. This thesis investigates this phenomenon, which can bring large amount of undue moisture within in the envelope assembly.

This thesis presents in detail the experimental work performed on large-scale wall assembly specimens to document their hygrothermal performance under conditions leading to inwards moisture flow. A large-scale experimental facility was utilized for the purpose of this work which consisted of weighing apparatuses to monitor the change of mass of the cladding and back-wall parts of wall specimens, a spraying array, a radiation array, and a test hut to provide controlled interior conditions. Five insulated wood-framed walls were monitored, four of which were brick cladded and one stucco cladded. Constructions of the backwalls varied by the material utilized for the exterior sheathing and the interior finish and also by presence or lack of an air cavity. The walls and the environment were equipped for electronic monitoring, complemented with manual weighing of gravimetric samples. The results of the experiments demonstrate that the presence of vapor tight interior finishes result in the accumulation of moisture in the

interior gypsum board. Furthermore, it is shown that even a vapor tight sheathing does not reduce sufficiently vapor flow to prevent moisture accumulation in the wood studs and the interior gypsum board. The highly positive effect of air space, and its ventilation, in reducing the magnitude of the inward vapor flow is shown.

During the process of studying the vapor diffusion through various wall assemblies, a vertical temperature and moisture content gradient was observed along the gypsum board-insulation interfaces. This phenomenon was also further investigated and studied both experimentally and numerically using CFD. The work indicated that stratification of humidity occurs within the insulation cavity of the wall.

This thesis demonstrates the mechanism of inward diffusion: under high thermal gradients, large amounts of vapor are transported, inducing high relative humidity against low-permeable layers in assemblies. By sorption, materials exposed to high relative humidity display high moisture content.

Acknowledgements

Working in the industry after completing my undergraduate studies never satisfied me enough. I always thought about continuing my studies but it didn't happen until I attended the 3rd International Building Physics Conference in Montreal in July 2006 to present my undergraduate thesis work. Listening to the interesting presentations, being among researchers and seeing how passionate one can be about a specific topic made me more confident that I want to be like them. The year after, I started my Masters studies.

Here I want to thank many people who helped and guided me through difference stages of my work. First in the list is of course my supervisor, Dr. Dominique Derome, who guided me through all stages of this work, from understanding the theory to construction of the specimens, measurement procedures and data analysis. Thanks to her, I was provided with the opportunity to be a part of an international project funded by ASHRAE. Also, as a part of this project, I got a chance to perform some CFD numerical studies. This was a big task for me as I was never exposed to computer simulations before. Many people helped me getting started with this CFD study and guided me through. I want to thank Dr. Bert Blocken, Adam Neil and Thijs Defraeye for spending their valuables times answering my questions and guiding me through this task.

The work I did at Concordia University would never be possible without the help and support of the faculty, stuff. I would like to thank the technicians at Concordia University, Luc Demers, Joe Hrib, and Rocco Lombardo for giving me a hand with anything I needed during my experimental work. Also I would like to thank Petr Slanina,

Philo Heijnen, Shereen Rifaat, Louis Cavanagh, Damien Courbe and Maher Ben Ali for helping me at various stages of my experimental work with construction of the specimen and taking measurements. I know it was not always fun to be stuck in the lab during a nice summer day. But I couldn't do this without your helps.

Last but not the least, I would like to thank my parents, Homa and Davoud Saneinejad, and my sister, Sheyda Saneinejad, for believing in me and always being there for me when I needed. I would like to dedicate this thesis to them as a small token of appreciation.

Like any other research work, this work did not always go easy and smooth. There were lots of ups and downs throughout both experimental as well as simulation works. In spite of all this, the satisfaction I experienced during this research work over weighed the challenging and hard times. I feel happy and proud to be able to call this piece of work, mine.

Table of Contents

List of Figures

List of Tables

Nomenclature

A	area	$[m^2]$
c_p	specific heat	[J/kg.K]
d	thickness	[m]
g	gravitational acceleration	$[m/s^2]$
h_c	convection heat transfer coefficient	$[W/m^2K]$
h_r	radiative heat transfer coefficient	$[W/m^2K]$
k	specific permeability	$[m^2]$
K	thermal conductivity coefficient	[W/m.K]
p	pressure	[Pa]
p_v	partial vapor pressure	[Pa]
q	heat flux	$[W/m^2]$
q_v	vapor flux though material	$[ng/m^2s]$
Q	volume flow	$[m^3/s]$
T	temperature	[K]
ΔT	temperature difference	[K]
z	elevation	[m]

Greek Alphabet Symbols

β	thermal expansion coefficient	[1/K]
ε	total emissivity coefficient	[-]
ρ	density	$[kg/m^3]$
σ	stephan-Boltzmann constant	$[W/m^2K^4]$
μ	dynamic viscosity	[kg/m.s]
ν	kinematic viscosity	$[m^2/s]$
δ	water vapor permeability	[ng/Pa.m.s]

Subscripts

c	convective
f	fluid

m	porous material
r	radiative
v	vapor

1 Introduction

Over the past few decades, attention to moisture control in building envelope has been increasing. One moisture transport occurrence that still needs to be studied and investigated is solar-driven vapor transport. This phenomenon occurs when a building with an absorptive cladding such as brick masonry is wetted by rain and then exposed to cyclic solar radiation. Such combination of rain and solar radiation loadings can result in inward vapor flow. Although this phenomenon is more prevalent is mixed and hot climates, it can be also observed during summer in cold climate zones.

Depending of the envelope composition, this inward flow can be restricted by vapor tight interior material layers such as polyethylene sheet used as vapor retarder, vinyl wall covering or alkyd-based paint. The eventual moisture accumulation within the wall can lead to problems ranging from rotting of the wood frame elements to formation of mold on the surface of interior finish of gypsum board. The presence of moisture can also reduce the thermal resistance of the insulating material and cause dimensional changes in wood framing elements.

Various studies have investigated the occurrence of solar-driven inward vapor flow, have identified problems resulting from such flow and, eventually, have suggested ways to eliminate it. However, the phenomenon of cyclic vapor flow driven by solar radiation and the influence of the wall composition on the hygrothermal performance and durability of wall systems subjected to such flow are not yet fully understood. It is therefore relevant to study the phenomenon of solar-driven inward vapor transport in more detail and investigate means to minimize its related risk.

1.1 Objectives

The main objective of the work presented in this thesis is:

- to provide a better understanding of the phenomenon of solar-driven vapor transport

The sub-objectives of this work are:

- to evaluate experimentally the performance of large-scale wall assemblies with different constructions subjected to inwards vapor flows and high thermal gradient,
- to model the moisture conditions with the wall undergoing inward moisture transport, and
- to provide guidelines and suggest strategies to eliminate or reduce risk associated with inwards vapor flow and to improve the overall performance of wall assemblies.

In particular, as vapor diffusion through various wall assemblies was studied, a vertical temperature and moisture content gradient was observed along the gypsum board-insulation interface. This unforeseen phenomenon was also further investigated and studied both experimentally and numerically.

1.2 Methodology

In order to investigate the phenomenon of solar driven vapor transport in detail, an experimental task was undertaken. The methodology of this work is noted below:

- Conditions suitable for inward vapor flows in large-scale wall assemblies were created by the means of a thoughtfully designed experimental set up. For this

purpose, the set-up was equipped with a spraying array, a radiation array, and a test hut to provide controlled interior conditions.

- In order to create an inward vapor flow though the specimen, the exterior cladding was initially wetted and then the specimen was exposed to 8 hours of simulated solar radiation. These conditions created a large vapor pressure on the exterior side of the specimen. With the interior side of the specimen being exposed to air conditioned indoor conditions, having a lower vapor pressure, a large vapor pressure gradient was created across the assembly. This vapor pressure gradient resulted in inwards vapor flows.
- Environmental conditions of the lab and the test hut were monitored during the test procedures using RH/temperature probes. This was done in order to allow comparison of the conditions within the wall with those at the boundaries and to understand patterns the of air/vapor flow better.
- Specimens with various compositions were built for the purpose of this study. Their constructions had similar structural wood frame in common, but varied in the material used for the interior finishes or the exterior sheathings, and also in lack or presence of an air cavity and its ventilation. For the purpose of this experiment, only one element of the wall was modified each time, in order to enable evaluating the effect of that single element on the performance of the assembly.
- In order to monitor the environmental conditions within the assemblies, the specimens were equipped with RH/temperature probes and thermocouples as various locations. RH/temperature probes were placed at the centre of the air

cavity and the insulation cavity. Thermocouples were installed at all possible interface at three different heights. This allowed monitoring the temperature along the height of the interfaces.

- Change of mass of the two main components of each specimen, i.e. the cladding and the back wall, were continuously recorded using a weight apparatus. This allowed for close monitoring of even small variations of the mass of these components and provided an efficient means for observing the accumulation of moisture resulting from inward vapor flow though the wall in different components.
- In addition to the continuous electronic mass monitoring of the specimens, manual weighing of gravimetric samples, taken from various components of the specimens, were performed. This allowed for close monitoring of the mass changes of those individual wall elements and enabled better understanding of the performance of the wall.
- Finally, after completion of each test, individual elements of the specimen were visually inspected. Inspection allowed for observing any mold growth or damages to the wall components and provided a tool for better understanding of the phenomenon of inwards vapor transport.

In addition to the experimental work performed to study solar driven vapor transport, numerical and experimental studies were undertaken to understand the pattern of air and moisture movements within the insulation cavity of the studied walls. The methodology of these experimental and numerical works is outlined blow.

First experimental test was performed to study the temperature profile in the insulation cavity of a wall.

- For the purpose of this study, the same test set-up used for the previous studies was utilized. High temperature gradient was imposed across the assembly by exposing it to simulated solar radiation on one side, and to air conditioned indoor condition on the other side. This temperature gradient resulted in heat flow and temperature profile in the insulation cavity.
- Detailed and close monitoring of the temperature profile in the insulation cavity used an array of thermocouples. This array of thermocouples was highly concentrated at the critical location of the cavity such as the top and bottom of the wall as well as areas beside the boundaries.

To study the temperature profile in the insulation cavity further, a numerical study was undertaken using CFD.

- A 2D mesh was created using meshing tool of GAMBIT, representing the stucco-cladded wall assembly. The density of the grid was higher at the critical locations of the wall being the top and bottom as well as areas close to boundaries. This provided a more detailed numerical calculation since the flow at these locations is more complex.
- Constant temperature conditions were imposed on the exterior and interior boundaries, exposing the wall to a large temperature gradient.
- A specific porosity and air permeability was assigned to the interior of the insulation cavity. This represented the fiber glass batt insulation.
- Calculations were performed using a laminar model.

- Temperature profile and air movement in the insulation cavity were studied using temperature contours and air velocity vectors.

A second experimental test was performed to study the relative humidity profile in the insulation cavity of a wall.

- In order to observe the relative humidity conditions in the insulation cavity, an inwards vapor flow was created across the assembly using the same procedures as was done for the study of inwards vapor flow.
- For this test, RH/temperature probes were installed within the test assembly, not only at mid-height, but at three different heights. This allowed vertical monitoring of the relative humidity and temperature profiles at these locations. In addition, monitoring of temperature at all interfaces though the specimen was enabled using thermocouples also installed at three different heights.

To study the moisture content profile in the insulation cavity further, a numerical study was undertaken using CFD.

- A 2D mesh which was created for the earlier simulation was utilized for this study.
- Constant temperature and relative humidity conditions were imposed on the interior and exterior boundary conditions, exposing the wall to a large temperature and vapor pressure gradient.
- A specific porosity and air permeability was assigned to the interior of the insulation cavity. This represented the fiber glass batt insulation.
- Calculations were performed using the species model to consider for the water vapor mixed with air, and a laminar viscous model.

- Temperature profile, vapor pressure profile and air movement in the insulation cavity were studied using temperature contours, vapor pressure contours and air velocity vectors.

1.3 Organization of the thesis

The thesis is organized in 5 chapters. The next chapter is a literature review that first presents the fundamentals of building envelope systems. Some basis of heat and mass transport, including natural convection in porous material is given in sections 2.3 to 2.5. Section 2.6 is a review of the previous studies on solar-driven vapor diffusion, and finally section 2.7 a review of previous studies on natural convection in porous material.

Chapter 3 contains the description of the experimental work undertaken to study solar-driven vapor transport. The experimental work presented in this thesis is one component of a larger research project, funded by ASHRAE (1235 TRP). Section 3.1 is a description of the experimental set-up i.e. the tested wall assemblies, environmental conditions and measurement protocol. Test procedures are explained in section 3.2. The achieved results are presented and analyzed in section 3.3 and comparative analysis is followed in section 3.4. This chapter ends with a conclusion of all performed studies in section 3.5.

Chapter 4 is a description of the experimental and numerical studies to understand the temperature and water vapor profile in the insulation cavity of a wall assembly. Sections 4.1 and 4.2 detail the experimental work undertaken to study the temperature, and water vapor profile, respectively. Section 4.3 describes the theoretical study of occurrence of convection loop in the insulation cavity. The numerical studies performed

to investigate the temperature profile and water vapor profile in the insulation cavity are presented in sections 4.4 and 4.5, respectively. Section 4.6 is a conclusion of this chapter.

Chapter 5 presents the guidelines delivered through this research study to designers and practitioners with the aim of improving the overall design and performance of buildings.

Finally chapter 6 presents the overall conclusion of this thesis, highlighting the main results and contributions of the work and discussing future work.

2 Literature review

2.1 Introduction

This literature review summarizes the current knowledge on solar-driven vapor diffusion. First, the building envelope system is presented. Then, the physical phenomena involved in solar-driven vapor transport are reviewed. Finally, a detailed review of previous work on solar driven moisture transport, for various wall compositions and geographical locations, gives the state-of-the art on the main topic of the thesis. A review of some investigations on natural convection in porous material completes this chapter.

2.2 Building envelope

A building envelope is the system separating the exterior and interior environments. It has to undertake a variety of loadings such as structural loads, as well as heat, air and moisture loads. An envelope usually consists of two main parts: an exterior cladding and an interior back wall. In this thesis, the focus is on the assemblies with an exterior cladding placed in front of the back wall whose main structural frame is light-weight wood construction. Three main types of assemblies were studied in this thesis. All contained an insulated wood frame. First assembly, shown in Figure 2.1a, had an exterior cladding of brick veneer and a conventional exterior sheathing (OSB). Next assembly, shown in Figure 2.1b, had an exterior cladding of brick and an exterior sheathing of XPS. The third assembly, shown in Figure 2.1c, had an exterior cladding of stucco.

by this insulating element, and/or by the insulation board placed outward of the stud (Figure 2.1b).

The wall framing is covered with "exterior sheathing" on the exterior side. This layer is placed to provide structural integrity for the framing. The material used for exterior sheathing can be hygroscopic such as OSB. Also it can be replaced with non-hygroscopic such as XPS. In this case, metal strips are fastened diagonally for bracing laterally the wood structure. If a hygroscopic sheathing is used, it is usually covered with a protective weather resistive barrier layer. This element, being the internal drainage layer, allows for shedding of rain water or condensation and eliminates wetting of the sheathing and water penetration into the assembly. The exterior sheathing, or its combination with the internal drainage layer, act as an air barrier. The purpose of air barrier is to control air movement due to pressure differences though the envelope which is one of the main sources of moisture transport.

The interior side of the wood framing is covered with an interior sheathing which is usually gypsum board. This layer provides an interior finish for the wall and is usually covered with a wall paper or paint.

Another element that is mostly seen in these types of walls is a vapor barrier. Water vapor passing though a wall assembly can damage the internal elements by condensing or getting absorbed by various materials. Therefore a vapor tight layer is usually placed within an assembly to control vapor flow. Placement of this layer in an envelope depends on the geographic location of the area where the building is located, being on the inside in cold climate area, or non existent in hot and humid environmental conditions. Intermediate solutions are needed for mixed climates.

2.3 Physics of heat transfer

Heat transfer can be achieved by three means: (1) Conduction, i.e. molecule to molecule, through solid objects; (2) Convection, by movement of fluid, i.e. air; (3) Radiation, through electromagnetic waves, between surfaces.

Conduction

Conduction is achieved through direct molecular contact, and in a building envelope it is the method by which the most heat flow occurs. Conduction heat flow relation is expressed by Fourier's law:

$$q = -\lambda \frac{dT}{dd} \tag{2.1}$$

where q – heat flux [W/m^2]

T– temperature [K]

d – thickness of the body [m]

λ – thermal conductivity coefficient [W/m.K]

Convection

Convection is another heat transfer mechanism described as heat transfer between a solid surface and the adjacent moving fluid. Convection heat transfer at the surface can be determined by:

$$q = h_c (T_{surface} - T_{fluid}) \tag{2.2}$$

where q – heat flux [W/m^2]

h_c – convection heat transfer coefficient [W/m^{2}K]

$T_{surface}$ – surface temperature of body [K]

T_{fluid} – temperature of fluid in contact with body [K]

Radiation

Radiation, as the third heat transfer mechanism, can be simplified to by assuming that the air temperature is equivalent to the temperature of the sky:

$$q = h_r (T_{surface} - T_{ambient-air}) \tag{2.3}$$

where q – heat flux [W/m^2]

h_r – radiative heat transfer coefficient [W/m^{2}K]

$T_{surface}$ – surface temperature of body [K]

$T_{ambient-air}$ – temperature of sky [K]

and

$$h_r = \frac{\varepsilon\sigma(T_{surface}^{\ 4} - T_{ambient-air}^{\ 4})}{(T_{surface} - T_{ambient-air})} \tag{2.4}$$

where ε – total emissivity coefficient

σ – Stephan-Boltzmann constant = 5.67 x 10^{-8} [W/m^{2}K^4]

2.4 Physics of natural convection in porous media

Natural convection is a result of air pressure difference due to buoyancy as opposed to forced convection that is caused by driving forces such as winds or fans. Temperature differences cause density difference which results in pressure difference:

$$P_1 - P_2 = \Delta\rho.g.z \tag{2.5}$$

where p – pressure [Pa]

ρ – density [kg/m^3]

g – gravitational acceleration [9.81 m/s^2]

z – elevation [m]

In this section, some basic notions of natural convection in a porous material are introduced and explained.

Specific permeability

Specific permeability is defied as the fluid conductivity of the porous material and this value is determined by the structure of the material. For insulation, permeability varies with direction of fibers and its density. Its dimension is m^2 and it is roughly a measure of the mean square pore diameter of the material.

Specific permeability (k) can be calculated by:

$$k = -\frac{Q}{A} \times \frac{\partial x}{\partial p} \times \mu \tag{2.6}$$

where Q – volume flow [m^3/s]

A – area [m^2]

μ – dynamic viscosity [kg/m.s]

p – pressure [Pa]

Values of specific permeability have been measured by various researchers for mineral wool insulation (Table 2.1). As it can be seen, the values vary with density and depend on the direction of the fibers in the insulation.

Table 2.1 *Reported mineral wool permeability values*

density (kg/m^3)	permeability (m^2)			author
	no direction mentioned	parallel	perpendicular	
6 – 8	1.47E-8 (loose fill)			Silberstein et al. (1990)
6 – 8	5.0E-8			Langlais et al. (1990)
6 – 9	5.0E-8 (glass fibre batt)			Silberstein et al. (1990)
9.4	4.0E-8 (loosefill)			Wahlgren (2002)
9.6		9.5E-9	6.8E-9	Dyrbol et al. (2002)
10	6.0E-9			Bankvall (1972)
11.1		6.5E-9	3.9E-9	Dyrbol et al. (2002)
15		9.0E-9	6.0E-9	Ciucasu et al (2005)
17		6.0E-9	3.2E-9	Kohonen et al. (1985)
18		6.0E-9	3.9E-9	Ciucasu et al (2005)
18.3		3.69E-9	1.86E-9	Økland (1998)
30		2.8E-9	1.7E-9	Dyrbol et al. (2002)
75	1.8E-9 (glass fibre batt)			Silberstein et al. (1990)
	0.75E-8 (mineral wool)			Shankar, Hagentoft, (2000)
	1.0E-8 (loose fill)			Shankar, Hagentoft, (2000)
	1.0E-8			Le Breton et al. (1991)

Figure 2.2 plots permeability versus density based on the gathered data presented in Table 2.1. The data shown with the same color are for the same density, but different directions of fibers (parallel vs. perpendicular). Air permeability parallel to direction of the fibers is higher than perpendicular. From this figure, the decrease of air permeability of the insulation with increasing density is clear.

where

$$\nu = \frac{\mu_f}{\rho_f} \tag{2.8}$$

and β – thermal expansion coefficient [1/K]

d – thickness of insulation [m]

k – specific permeability [m^2]

ν – kinematic viscosity [m^2/s]

Cp_f – specific heat [J/kg.K]

ρ_f – density [kg/m^3]

μ_f – dynamic viscosity [kg/m.s]

and the subscripts "f" and "m" identify fluid and porous material, respectively.

When Ra_o is below a critical value, heat transfer is primarily under the form of conduction. When it exceeds the critical value, heat transfer is primarily in form of convection. This critical value can be used as an indication of occurrence of a significant level of natural convection where it can affect the thermal values of the insulation, although even at Ra_o values below this critical level, natural convection can occur. The value of the critical Ra_o number depends on the boundary conditions, density of the insulation, and direction air flow (horizontal or vertical). For insulation placed vertically, different, but very close values of critical Ra_o are reported. Bankvall (1972) reports a critical Ra_o of approximately 4 to 6 for aspect ratio h/d ratio of 1 to 10 and this value increases as aspect ratio increases, reaching approximately 20 for h/d of 50. This is shown in Figure 2.3 below.

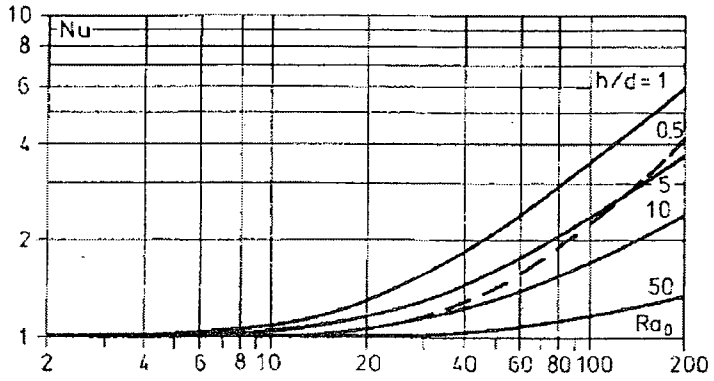

Fig. 2.3 Reported values of critical porous Rayleigh number, graph from Bankvall (1972)

Schneider (1963) has reported a critical Ra_o value of 6 for aspect ratio of 7.5 which is similar to the results of Bankvall, 1972. Also a value of 5 is reported by Kohonen et al. (1985) for aspect ratio of 7.33.

Nusselt number

The ratio of convective to conductive heat transfer is used to describe thermal influence of convection air flows. This ratio is called Nusselt number. Nusselt number (Nu) is a function of Ra_o and aspect ratio, and where no convective flow is present, Nu equals to one.

Aspect ratio

Aspect ratio is the ratio of height (h) to depth (d) of the cavity containing the porous material (Figure 2.4). Aspect ratio affects the critical Rayleigh number and eventually the onset of natural convection. Studies of Bankvall (1972) shows that the higher the aspect ratio is the less is the natural convection/ heat transfer (Refer to Fig 2.1 above). This is explained by the convective flow from one vertical side to the other at the top and at the bottom of the space. For spaces with large aspect ratio (high spaces), the end region flow will influence a relatively small part of the total space (Bankvall, 1972).

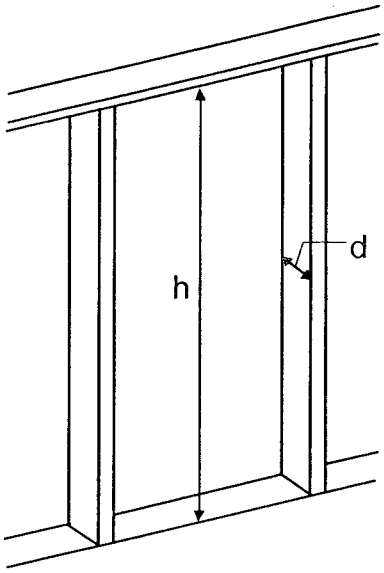

Fig. 2.4 Schematic representation of a cavity showing height (h) and depth (d)

2.5 Physics of mass transfer

Moisture can move through a building envelope in two forms: gas and liquid. Three main methods transfer moisture though a system: capillary action, for moisture in liquid form; and convection, and vapor diffusion for water vapor.

Capillary action

Capillary action moves liquid water through the pores of materials. Capillary action is more important in material with small pores as the size of the pores governs the rate and strength of suction. Capillary action is often a concern when a material is in contact with liquid water or a material that is close to saturation.

Convection

Moving air through the building envelope can carry moisture with it and distribute it within the envelope assembly. One of the causes of air movement is pressure differential due to temperature difference (stack effect). The higher the temperature of air,

the higher its saturation vapor pressure and hence at a constant relative humidity, the higher its vapor pressure will be. Saturation vapor pressure as a function of temperature is shown in the figure below. Some other causes of air movement are mechanical system, wind, etc.

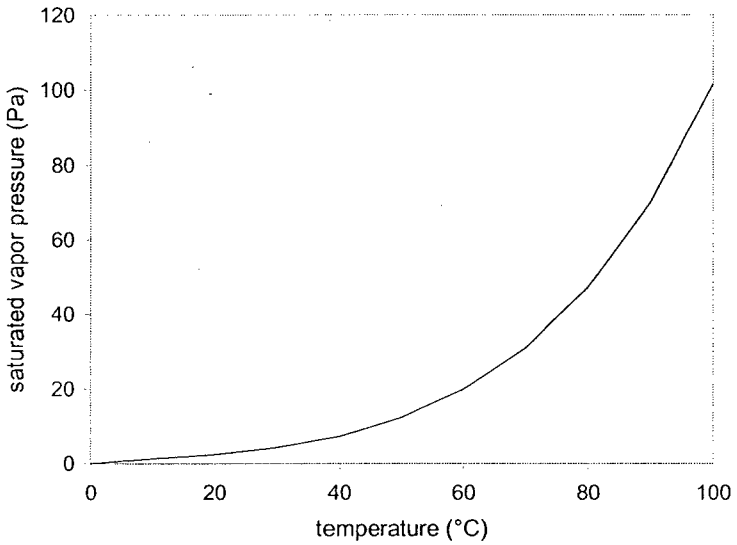

Fig. 2.5 Saturation vapor pressure versus temperature

Vapor diffusion

Vapor diffusion is the movement of moisture in the vapor state through a material as a result of a vapor pressure difference. In this case, water vapor diffuses from areas with higher concentration to areas with lower concentration.

All materials show some sort of resistance to this vapor transport mechanism; the material property is known as the material's water vapor permeability. Low permeability allows little vapor diffusion through, while a high permeability does not offer much resistance to vapor flow. Low permeable materials, also known as vapor tight, such as polyethylene sheet, are often used as vapor barriers. High permeable materials are

referred to as vapor open. Permeance is stated in ng/s.m.Pa in Canada. The SI unit is equivalent to 0.017 US perms.

Diffusion of water through a material is expressed using Fick's law:

$$q_V = -\delta(\frac{dp_v}{dx}) \tag{2.9}$$

where q_v – vapor flux though material [ng/m^{2}s]

dp_v – partial vapor pressure [Pa]

x – distance along flow path [m]

δ – water vapor permeability [ng/Pa.m.s]

2.6 Solar-driven vapor transport

Solar driven vapor transport is a phenomenon which happens in presence of a wet cladding and solar radiation. The wet, heated cladding dries resulting in a high vapor pressure behind the cladding. As the interior vapor pressure is much lower, vapor flows inwards. Depending on the wall assembly, moisture flow can be retarded and lead to undue moisture accumulation which could cause interstitial condensation on the surface of a vapor tight interior finish (or interior vapor barrier). A lot of previous studies look at winter condensation which may occur during outward flow of humid indoor air. Less attention has been paid to inward flow, while it could have worse consequences than the ones caused by outward vapor flow depending on the constructions and the climate conditions. Some studies have been done on solar-driven vapor transport and ways to eliminate it. The following section is a review of the previous works on this topic.

2.6.1 Solar-driven vapor transport studies

Inward vapor transport has been the subject of some study by various researchers over the last 50 years. Although inwards vapor flow can occur on a sustained basis in regions with hot and humid climate especially when the interior areas are air-conditioned, the most studied situation is the inward vapor transport observed during hot summers of cold climate areas.

Inwards solar-driven vapor flow can be severe due to the high surface temperature of the exterior cladding, creating a larger vapor pressure gradient across the assembly. In this section, research works which observe the solar-driven vapor flow are discussed. In the next section, recommended strategies suggested by various researchers are presented.

Wilson (1965) is one of the first researchers to have studied solar-driven vapor transport, and he did so in Ottawa, Canada. He studied the behavior of insulated masonry panels with an interior vapor barrier, during summer. He observed extensive amount of summer condensation against the vapor barrier when the assembly had no air space and this amount was reduced when an air space was provided.

Sherwood (1985) studied the effect of summer condensation in a field testing in hot and humid weather of Gulfport, Mississippi with maximum summer temperature of 37°C. He observed high amount of moisture on the assemblies facing south and with hygroscopic exterior sheathing.

TenWolde and Mei (1985) tested various wall assemblies in Lamar University, Beaumont, TX with summer temperature ranging from 20°C to 35 °C with extremely high relative humidity ranging from 60% to 80%. Cyclic condensation was observed in assemblies with exterior permeable sheathing and interior polyethylene vapor retarder.

Southern (1986) investigated occurrence of summer condensation in a series of test walls constructed in East Kilbride, Scotland. The walls were composed of exterior concrete block against which insulation material was placed, followed by a 25mm air gap and wood battens which were covered with a layer of 500 gauge polyethylene sheet. The test assemblies were exposed to air conditioned interiors. Test results showed that from the end of May until early October, the assemblies experienced condensation on the exterior surface of polyethylene sheet. Measuring the moisture content of the wood battens at the end of the test period showed that some battens were wet enough for rot to develop, indicating the risk associated with summer condensation. Southern concludes that condensation on the back of the vapor retarder can occur under natural weather conditions which is mainly influenced by solar heating of the wall surface, coupled with a cooler internal room temperature.

Andersen (1987) conducted a full-year test on a wall composition in Denmark, consisting of exterior brick cladding and interior vapor barrier. When the interior space was unheated, condensation was observed and the moisture content of the wood framing reached 28% by the end of summer. Andersen believed that such construction would be in serious danger for fungus attack and cannot be recommended.

Sandin (1993) studied solar vapor transport in Sweden during summer. An experimental work was performed for natural indoor climate. It was observed that the assembly with a 20mm air space and an inner vapor barrier experienced a 100% relative humidity in the mineral wool. This amount was reduced by widening the air space and removing the inner vapor barrier.

Straube and Burnett (1995) field tested a number of assemblies at University of Waterloo. Results showed inward vapor flow especially in assemblies with exterior fiberglass sheathing. The authors indicate that the daily heating effects, when associated with moisture trapped behind vapor impermeable cladding, can produce large, short-term inward vapor drives whose magnitude can greatly exceed those outward-acting vapor pressure differences in winter. These inward drives can cause condensation on the inner vapor barrier, especially in air-conditioned buildings. In another study by Straube and Burnett (1998) in Waterloo, Canada, summer condensation was observed and it was more severe in the assemblies with vapor open exterior sheathing.

Wilkinson et al. (2007) conducted a series of testing in field exposure facility of University of Waterloo to study the occurrence of summer condensation in various wall compositions. Test results showed elevated moisture levels, especially toward the interior surface, for the assemblies with interior vapor barrier. Evidence of condensation and rundown on the surface of the vapor barrier of the south wall was observed.

In addition to these field studies, a number of studies have been undertaken using laboratory experiments and computer simulations, to study the occurrence of solar vapor transport in wall assemblies further.

Kan (2002) performed a series of laboratory testing at University of Toronto to study the effect of summer solar driven vapor with surface cladding temperature reaching 43°C. Assemblies with various configurations were tested. High moisture accumulation was observed in the assemblies with no air space and no XPS (vapor tight exterior sheathing). The test conditions were simulated using a heat and moisture transport code,

MOIST. MOIST simulation results showed higher moisture conditions than laboratory results and theoretically predicated quantities, but it remained within the same magnitude.

Pressnail et al. (2003) studied the effect of summer condensation in a series of laboratory testing using the same test set-up as used by Kan (2002). Assemblies with various constructions were tested. It was observed that high amount of moisture accumulated in the assemblies with lower permeable exterior sheathing. The amount of moisture gain was reduced, but still existed, when testing the assembly with vapor tight XPS sheathing.

The findings of the works listed above are summarized next.

2.6.2 Factors affecting solar-driven vapor transport

Researchers have evaluated assemblies with different construction in terms of their behavior in the case of solar-driven vapor flow. A number of strategies have been suggested to be beneficial to minimize the risk associated with inwards vapor flow. These influencing factors are:

- vapor permeance of the interior finish (vapor barrier)
- air cavity and ventilation behind the cladding
- vapor permeance of the exterior sheathing
- material properties of the cladding
- interior environment conditions

In this section we look at how researchers have investigated these parameters and what recommendation they made to eliminate the problems associated with inwards vapor flow.

Vapor permeance of the interior finish (vapor barrier)

As a strategy in eliminating inwards vapor flow, some researchers have suggested eliminating the vapor tight interior finish, although not all studies agree on the effectiveness of this strategy. In this section, the works in which the effect of the vapor tight interior finish has been studied are presented.

Researchers such as TenWolde and Mei (1985) and Karagiozis et al. (2001) have studied the effect of having a vapor tight interior layer on vapor flow though wall assemblies in hot and humid climates both through field tests and numerical modeling. TenWolde and Mei (1985) observed cyclic condensation in assemblies with interior vapor retarder, and completely dry assemblies when they had no vapor retarder. Karagiozis et al. (2001) using the advanced HAM transport code, LATENITE 3.0 VTT, found slower drying rates of the walls with interior vapor retarder of paint. This study also assessed the risk of mold growth on the exterior face of vapor retarder and fount it to be high in such walls. It is suggested that an interior vapor retarder should not be used unless one is also present on the exterior side (TenWolde and Mei, 1985).

Wilkinson et al. (2007) evaluated the effect of interior vapor barrier on the performance of the walls in an area with cold climate (University of Waterloo) through field testing. Their results supported the conclusion of the previous studies done in hot and humid climates, showing an elevated moisture levels, especially toward the interior surface, for the assemblies with interior vapor barrier. Relative humidity in the stud space was measured to be between 80% to 100% during summer and these walls were in the risk of condensation for 908 hours during summer in 91 days. This was much higher than

the risk of condensation of only 15 hours in 91 days for walls with no interior vapor barrier.

Sandin (1993) also supported the idea that one of the ways to reduce the vapor transport from the masonry to the interior is to ensure the moisture transport can take place through the wall without any obstructions by avoiding using an inner vapor barrier. In his studies, he observed that an assembly with a 20mm air space and an inner vapor barrier experienced a 100% relative humidity in the mineral wool. This level of relative humidity was reduced to 85% when the inner vapor barrier was removed.

Using a vapor retarder with variable permeance was suggested by Kunzel (1999) to control vapor flow in both winter and summer conditions. Such vapor retarder acts like a conventional vapor retarder at the interior side of an assembly during the cold season where humidity conditions are relatively low. However when exposed to high relative humidity levels, the membrane becomes very permeable. Its vapor permeability is shown in Figure 2.6 as a function of relative humidity. The graph shows that, at a relative humidity below 50%, the retarder acts like a vapor retarder. However, above 90% relative humidity, the film becomes vapor permeable. Studies conducted by Kunzel (1999) showed the efficiency of such material when tested in an unvented cathedral ceiling, by reducing the moisture damages risk in the building envelope.

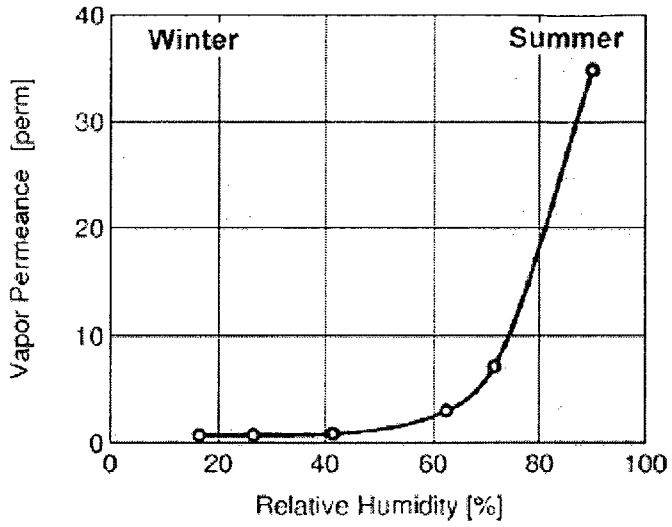

Fig. 2.6 Permeability of vapor retarder with variable permeance (from Kunzel, 1999)

Further, to show the efficiency of the above mentioned vapor retarder, Kunzel (2005) looked at the phenomena of solar driven vapor transport as a drying mechanism for moisture that was driven inside during cold winter months for the cold and northern costal climates of US as well as similar climate zones in Europe and Canada, using advanced heat and moisture transport code WUFI. They observed that even when a moderate vapor barrier (57 ng/Pa.m.s or 1 perm) was used on the interior side of the assembly, the amount of moisture that entered the assembly during winter was higher than what was dried out in summer. It was suggested that either a low-perm retarder (permeance < 6 ng/Pa.m.s or 0.1 perm), or the humidity controlled vapor retarder be used.

Although most of the works discussed up to now showed the effectiveness of having a high permeance interior finish (vapor barrier), or even eliminating this vapor impermeable layer, in reducing the risks associated with inwards vapor flows, Lawton and Brown (2003) found otherwise. Through numerical studies on a number of assemblies in the temperate climates of British Columbia and the northwestern United

States, using the HAM transport code hygIRC, they showed that deleting the interior vapor barrier and allow drying to the inside was not always that beneficial. Their results showed that the assemblies finished with paint of various permeabilities on the interior experienced higher gypsum board moisture content than the assemblies with polyethylene vapor barrier or no vapor barrier on the interior. They argued that a good reason to be cautious about deleting a polyethylene vapor barrier and relying on drying to the inside was that the paper-faced gypsum board is very sensitive to moisture exposure, and exposure to high humidity or small quantities of liquid water creates conditions that often lead to mold growth on the paper facing. They believed that vapor barrier on the interior side of the assembly could protect gypsum board from being exposed to high amount of moisture.

The presence of a vapor tight membrane on the interior of an envelope is a topic of controversy when considering inwards vapor flow. Although most researchers have shown the disadvantages of its existence, some still believe it can be beneficial. TenWolde & Mei (1985), Sandin (1993), and Wilkinson et al. (2007) have show how an interior vapor tight membrane can be problematic and will result in some levels of inwards vapor flow. Karagiozis et al. (2001) have studied how an interior vapor retarder reduces the drying rates of a wall. Knowing the disadvantage of an interior vapor tight membrane, Kunzel (1999) suggest using smart vapor retarder which can eliminate both summer and winter condensations. Contrary to these studies, Lawton & Brown (2002) suggest that a vapor barrier on the interior side of the assembly can be beneficial in cold climates by protecting the gypsum board from being exposed to high amount of moisture.

Air cavity and ventilation behind cladding

The presence of an air cavity behind the cladding, and particularly when it is ventilated, is found to be effective in reducing the risks associated with inwards vapor flows. In this section, some studies in which this matter is investigated are presented.

Effect of an air space and its ventilation, in reducing vapor transport towards inside is studied by Wilson (1965), Kan (2002), and Pressnail et al. (2003). They all studied assemblies, first with no air space at all, then with an air space and further with a ventilated air space. All studies concluded that while significant wetting can be observed in assemblies with no air space, providing an air space, even if non-vented, reduces the risk of wetting. Kan (2002) argued that the presence of air space, even if unvented, provides paths of air movement between outside and air space, acting like ventilation. Also all studies showed that a ventilated air space is the best strategy. Kan (2002)'s laboratory testing showed that even in an assembly with no exterior vapor control such as an XPS sheathing, no moisture gain was observed when a vented air space was present. Also Wilson (1965) showed that ventilating the air space eliminated the occurrence of condensation leaving the framing with a moisture content of 15%. This is due to lower temperature behind the sheathing in the case of ventilated cavity compared to a non-ventilated one, resulting in smaller inward vapor drive (Kan, 2002).

In support of the idea that the ventilated air cavity has as better performance in comparison to the absence of cavity or non ventilating it, Southern (1986) and Straube and Burnett (1998)'s studies both showed that assemblies with a ventilated air cavity had a marked reduction in the amount of condensation, or perform better in controlling inward summer vapor flows.

In addition to studying the effect of an air space, Sandin (1993) studied how widening the size of the air space could affect the behavior of the wall. He observed that the assembly with a 20mm air space and no inner vapor barrier experienced an 85% relative humidity in the mineral wool. This level of relative humidity was reduced to 50% when the size of the air space was increased to 50mm.

As we saw above, the effect of an air cavity, its size and its ventilation, on controlling inwards moisture flow has been studied by various researchers. All the above mentioned studies have shown that an air space, especially when it is ventilated, helps to reduce or eliminate the risks associated with inwards vapor flow.

Vapor permeance of the exterior sheathing

Installation of a vapor tight exterior sheathing is thought to be one of the strategies in reducing inward driven vapor flow. Although this is shown by many researchers through numerical and experimental studies, some researchers show otherwise. This section is a review of the works performed on this topic and presents the results of those works.

Researchers such as Sherwood (1985), Southern (1986), Straube and Burnett (1995) and Pressnail et al. (2003) have done comparative studies on assemblies with exterior sheathings made of various materials and permeabilities. The effect of more permeable exterior sheathings such as glass fiber insulation boards and vapor tight sheathings such as extruded polystyrene insulation (XPS) or expanded polystyrene insulation (EPS), on reducing vapor flow though wall assemblies have been studied. All studies showed that assemblies with a vapor open sheathing experienced higher amount of moisture, and even some levels of condensation, and this was even more extensive if

the assembly was exposed to higher intensity solar radiation, i.e. south wall (Sherwood,1985). Lower levels of moisture were observed, and occurrence of condensation was delayed in the walls with vapor tight exterior sheathing (Pressnail et al., 2003). The importance of having sealed joints between the sheets of exterior sheathing was highlighted by Southern (1986). He showed that even when an exterior sheathing had very low vapor permeability, it still did not eliminate condensation when gaps were present between the joints of the boards. This will allow water vapor to transfer through the assembly.

While Wilkinson et al. (2007) showed the minimal risk of condensation in the assemblies with XPS exterior sheathing through their field testing at University of Waterloo, Kan (2002)'s laboratory testing at University of Toronto indicated that when XPS sheathing was used, even when no air gap was present, no moisture accumulation in the wall assemblies was observed.

Although all the above noted studies supported the idea that a vapor tight exterior sheathing reduces the risks associated with inwards vapor flow, Karagiozis et al. (2001) showed that this vapor tight exterior sheathing can have a negative effect on the drying rate of the walls in hot and humid climates. Their studies, using the advanced HAM transport code, LATENITE 3.0 VTT, showed that although the exterior sheathing of EPS had some thermal benefits, it retarded the drying performance of the building envelope due to its low vapor permeability and the walls containing the EPS experienced higher moisture content.

Different studies have evaluated performance of the walls with a vapor tight layer on the exterior side. Sherwood (1985), Southern (1986), Straube & Burnett (1995),

Wilkinson et al. (2007), Kan (2002), and Pressnail et al. (2003) all agree that presence of a vapor tight exterior sheathing such as XPS prevents entry of moisture inside the wall assembly which could eventually cause condensation. Contrary to these studies, Karagiozis et al. (2001) does not find this exterior vapor tight layer advantageous. His study shows that an exterior vapor tight sheathing in hot and humid climates may retard the drying performance of the building envelope.

Material properties of the cladding

The material properties of the cladding, i.e. specifically the water uptake properties, can affect the amount of moisture that is driven inside a wall assembly. In this section, some studies in which attention has been paid to this influencing factor are presented.

Sandin (1993) believed that the relative humidity in the stud wall during summer was dependent on the vapor transport from the masonry to the interior and one of the ways to reduce this humidity was by keeping the masonry dry using water-repellent impregnation. Through his studies, he observed that the assembly with a 20mm air space and an inner vapor barrier experiences a 100% relative humidity in the mineral wool. This level of relative humidity was reduced to 85% by removing the inner vapor barrier, and was reduced even further to 45% when also the cladding was treated with water repellent impregnation. This showed the effect of less absorptive cladding in reducing inward vapor flow.

Hubbs and Hircock (2002) monitored a number of buildings with various exterior claddings and wall constructions in Vancouver, BC. They note that the buildings with porous stucco cladding experienced higher vapor pressure on the exterior surface of

vapor barrier than the building with vinyl cladding. They argued that this different was due to the fact that vinyl cladding was more resistant to inward vapor drive and also because the surface temperature of the stucco cladding reached much higher values, creating a bigger temperature flux and eventually vapor flux toward inside.

Both these studies agree that by lowering the water uptake of the material used as the exterior cladding, inward vapor drives are reduced, which results in reducing risks associated with this flow.

Interior environment conditions

Environmental condition of interior space is believed to affect the magnitude of the vapor pressure gradient across the assembly, which as a result, affect the magnitude vapor drive towards inside. To investigate this matter further, Andersen (1987) compared the performance of the assemblies with heated and unheated interior spaces. His test results showed that when the interior space was unheated, condensation was observed and the moisture content of the wood framing reached 28% by the end of summer. The moisture content of wood framing was reduced when the test was repeated for a heated interior space but it still reached 20% at times and condensation was observed for duration of three weeks.

2.7 Natural convection in porous media studies

Occurrence of natural convection in insulation material has been the subject of study by many researchers. Researches have looked at onset of natural convection and whether or not it will affect the conductivity of the insulation material. Studies have been done on both vertically and horizontally placed insulations. In this study we only focus

on the studies done on vertical configurations. The purpose of this literature review is to see whether these studies have observed a critical convection loop in the insulation cavity that could lead to a vertical temperature gradient on the two interfaces of the cavity.

Bankvall (1972) investigated the effect of natural convection on heat transfer insulated structures. Experiments were conducted on a wall structure 5.4m high and 3.5m wide, where a space of 1.5 m x 0.6 m was studied in detail. Insulations with densities of 10 to 60 kg/m^3 and thicknesses of 0.05 to 0.145 m were used. Temperature at the warm side was between 15°C to 20°C and at the cold side between -25°C to 5°C. As part of this study, the temperature field in the insulation cavity was observed. Measurements for some of the low density materials did not reveal any distortion of the temperature field inside the insulation cavity, which would be a characteristic of natural convective air flow. Also the porous Rayleigh number was measured to be 5 for a case where d = 0.145m, ΔT=35°C, ρ=12kg/m^3 and k(‖)= 1.1E-8m^2. This value of Ra_o, according the previous measurements in the same study, is theoretically not enough to create a significant convection loop.

Kohonen et al. (1985) investigated the effect of air flows (natural convection) in building structures numerically using the CCC2D computer code (coupled convection and conduction in 2D). The structure simulated was 2.2m high and 300mm thick space of fibrous insulating material in one-dimensional, horizontal temperature field. The constant air temperatures on the cold and warm sides of the wall were -20 and +20 °C, respectively. The insulation material was light-weight mineral wool with density of 17kg/m^3 and air permeability of 3.2E-9 m^2, perpendicular to fibers, and 6.0E-9 m^2, parallel to fibers. The porous Rayleigh number was calculated to be 5.2 for the closed

structure. The value of Ra_o was slightly above the critical value of 5 measured in the same study. The authors indicated that the values calculated for Ra_o did not mean that convection was absent, but that the average heat flow corresponded to pure conduction heat flow. The simulations showed that the flow field formed a circle, with the maximum magnitude of the velocity vector being approximately 0.25 mm/s. The vertical temperature profile showed slight bend in the upper and lower parts of the structure.

Okland (1998) studied occurrence of natural convection in highly-insulated building structures. The tested wall system had dimensions of 1.2m x 2.4m and was 0.3m thick, filled with fiberglass insulation batts (density of 18 kg/m^3 and air permeability of 1.86E-9 m^2 in perpendicular direction, and 3.69E-9 m^2 in parallel direction). A vapor barrier was present on the warm side of the assembly. The temperature on warm side was 23°C while the cold side was exposed to 0°C for first 15 days, and then -15°C for next 40 days. Built-in moisture was included in the insulation. For a completely insulated assembly, the modified Ra number was 3.5, which would normally not lead to a significant influence of natural convection. The relative humidity was slightly higher in the upper part of the wall compared to the lower part. The author believed that this could be explained by natural convection. Simulation was performed using the advanced HAM transport code, LATENITE. Good agreement was found between measurements and simulations. The flow field was observed to form a circular pattern with the maximum velocity being 0.16mm/s in the insulation cavity. Simulation also showed relative humidity and temperature iso-lines to deviate from a vertical plan at the top and the bottom which author believed could be the influence of natural convection.

Dyrbol et al. (2002) investigated the effect of natural convection on heat transfer in mineral wool, both experimentally and numerically, using the computer code, CHConP. Three different mineral wool insulation were tested: batt mineral wool with density of 30 kg/m^3 (MW1) and permeability of 1.7E-9 m^2, roll mineral wool with density of 9.6kg/m^3 (MW2) and permeability of 6.8E-9 m^2, and roll mineral wool with density of 11.1kg/m^3 (MW3) and permeability of 3.9E-9 m^2. These materials were tested for various thicknesses as well as with various temperature differences across them. Results showed that when the lowest permeable MW1 was tested, although no significant increase in the overall average heat flow was occurred, but distribution of heat flow across the height of the specimen was observed. This showed that natural convection could occur even with small temperature difference of only 20°C across the assembly. With MW2 and MW3, the average Nu numbers in the vertical positions increased with the temperature difference and with the specimen thickness. Permeability of MW3 seemed to be close to the limit for onset of natural convection. This paper concluded that the risk of convection increasing the total heat flow in the material was related to highly permeable materials (corresponding with low density) although both measurements and the matching computations showed a clear convection-induced redistribution of the heat flow in the material.

From the above studies, one can see that except for Bankvall (1972)'s study, in which no deviation on temperature on the interfaces of the insulation was observed, the rest of the studies, Kohonen et al. (1985), Dyrbol et al. (2002), and Okland (1998), observed some sort of increase of temperature or relative humidity with the height, in the insulation cavity. These researchers believed that the observed vertical temperature or

relative humidity gradient could be due to occurrence of natural convection in the insulation cavity, although the purpose of these studies was not to investigate the cause of this gradient.

2.8 Conclusion

From the review of the literature above, it can be observed that the phenomenon of inwards vapor transport has been identified and studies by various researchers. Studies have investigated occurrence of this phenomenon both in hot and humid, and cold climate areas. Various strategies have been suggested by researchers although not all studies agree on the effectiveness of each.

So far, most of the work done on inwards vapor transport aimed at reporting the occurrence of inward moisture movement due to the high temperature gradient. However, these works are limited in scope and data produced. Cyclic vapor flow driven by solar radiation and the influence of the wall composition on the hygrothermal performance and durability of wall systems subjected to such flow is a phenomenon that is not yet fully understood. Also heat and moisture profiles in the insulation cavity of assemblies exposed to inward moisture flows, and whether or not a convective air movement or air stratification occurs in the insulation cavity of such assemblies, needs to be studied in more detail. This thesis is a more extensive study of these phenomena.

Next chapter explains the experimental study undertaken in controlled laboratory conditions on large-scale wall specimens subjected to simulated wetting and solar radiation. The experimental set-up, test procedures, and experimental results are presented and the achieved results from various specimens are analyzed and compared to one another.

3 Experimental study of solar-driven vapor transport

The experimental work undertaken to study the performance of the wall assemblies subjected to inward vapor diffusion is explained in this chapter. Section 3.1 describes the experimental set-up used for the purpose of these experiments in detail. This includes description of the five tested wall specimens, the environmental conditions, and measurement protocol. Section 3.2 contains information about the test procedures. The achieved results are presented and analyzed in section 3.3. This is followed by a comparative analysis in section 3.4 and a general conclusion about this experimental study in section 3.5.

3.1 Experimental set-up

This section describes an existing experimental setup developed, as presented in Edelstein (2007), to perform the large-scale tests. The setup is designed to subject wall assemblies to simulated rain and sun exposure, while monitoring the changes of mass of the whole cladding and back-wall. Figure 3.1 shows a schematic representation of the test setup. This figure includes the radiation box, placed in front of the test specimen. The tested wall assembly is located between the radiation box and the test hut, and hung, with the weighing mechanism, from the gantry crane. The weighing mechanisms are partly represented by the two counter weights, the leaver arms and the two parts of the test specimen. The wall specimen is placed against an air-conditioned test hut that provides

3.1.3 Measurement protocol

To document the behavior of the wall specimens during the tests, an array of measurements on the wall specimens and in the environment was performed. The following sections explain the method of electronic and gravimetric monitoring of the individual specimen, the method of monitoring the environmental conditions and the description of the instruments used for the purpose of the monitoring.

3.1.3.1 Specimen monitoring

The specimen monitoring consisted of continuous monitoring of the whole mass of the individual brick wall, backwall or the entire stucco assembly, and periodic gravimetric measurements.

3.1.3.1.3 Whole mass continuous monitoring

The brick wall and the backwall (or the entire assembly in case of the stucco wall) were separately and continuously weighed during the test using a weighing system. Each weighing system was suspended from a gantry crane and consisted of a friction-free leaver arm supporting, at one end, a specimen and, at its other end, a counter-weight. A load cell was anchored between the counter weight and the floor and measured any mass change of the specimen during the test period. Figure 3.10 shows the overall weighing apparatus. A detailed description of the weighing apparatus is given in Appendix B.4.

Regarding the conditions on each side of the set-up, the temperature at the interior of the hut was kept constant at 16°C while the relative humidity was quite unsteady and varied between 45% and 85%. The temperature outside the radiation box varied during each wetting/drying cycle, reaching a maximum of approximately 42°C. The minima and maxima relative humidity levels on the outside varied a lot throughout the test period, reaching lows of 9% and highs of 50%. In terms of the ambient conditions of the whole experimental set-up, the temperature of the lab was usually around 24°C while the relative humidity varied between 25% and 57%.

3.3.1.2 Temperature and relative humidity across wall 1

The relative humidity and temperature at the centre of the air cavity and close to the gypsum board in the insulation cavity are shown in Figures 3.25 and 3.26.

The temperature in the air cavity varied with each test cycle. The range of minimum and maximum temperatures in the air cavity was approximately 30°C during the cyclic wetting/drying phase, while it increases to 35°C during the drying phase reaching a temperature of 60°C at its maximum value. The relative humidity in the air cavity also varied with each test cycle. At the beginning of the experiment, the maximum relative humidity and also the bracket between the minimum and maximum levels was quite high. During the wetting stage, the relative humidity reached a maximum value of 91%. The magnitude of variations in relative humidity as well as its average value started to decrease after the start of the drying phase. By the end of the drying phase, the maximum relative humidity was 20%.

temperature increased when the cyclic wetting was stopped and the wall exposed to radiation only, reaching a maximum of 75°C.

On the interior surface of the brick veneer, the maximum surface temperature increased by approximately 2°C after the wetting phase was terminated and the drying phase was started. The maximum temperature on this surface was 65°C.

The surface temperature behavior observed on the first two surfaces (increase of the maximum surface temperature after start of the drying phase) was also seen on the exterior and interior surfaces of OSB. The maximum surface temperature on the exterior surface of OSB was 65°C and on the interior surface of OSB is 62°C. A vertical temperature gradient was observed for the first instance at the exterior surface of the OSB and is repeated through the other inward layers on the wall. The range between the lowest and the highest surface temperatures on both the exterior and interior surfaces of OSB was approximately 10°C.

The temperature gradient that was observed on the surfaces of OSB continued to the exterior and interior surfaces of the gypsum board as well. This temperature gradient was approximately of 2°C on both interior and exterior surfaces of gypsum board.

3.3.1.3 Vapor pressure across wall 1

Figure 3.28 below shows the vapor pressure in the insulation cavity, air cavity and interior of the hut of this test specimen. Figure 3.29 shows the differential vapor pressure between the air cavity and insulation cavity, and between the insulation cavity and inside the hut.

sample reached a maximum moisture content of 46 kg/m^3 with an increase of 15 kg/m^3 during the entire test period, and the bottom sample reached a maximum moisture content of 42 kg/m^3 with an increase of approximately 8 kg/m^3 compared to its initial moisture content.

3.3.2 Test results of wall 2 (brick/paint)

This wall was constructed of exterior brick veneer cladding and interior backwall with OSB exterior sheathing and gypsum board covered with acrylic paint (instead of VWC as used in wall 1). The air cavity in this test was not vented. This test was performed for 20 days, from October 2, 2007 to October 22, 2007, including 14 days of cycling wetting and drying periods, and 6 days of drying. Appendix E presents the graphs plotted from the measured data from testing this assembly.

3.3.2.1 Environmental conditions

In this section, the environmental conditions on the indoor and outdoor of the tested assemblies and ambient laboratory of the laboratory are reported (Figures 3.33 and 3.34). No data of the outdoor relative humidity and temperature was recorded on day 6 of the measurements. This is due to malfunctioning of the RH probe during that day.

On the interior surface of the brick veneer, the maximum surface temperature increased by approximately 4°C after the wetting phase was terminated and the drying phase was started. The maximum temperature on this surface was 65°C.

The surface temperature behavior observed on the first two surfaces (increase of the maximum surface temperature after start of the drying phase) was also seen on the exterior and interior surfaces of OSB. The maximum surface temperature on the exterior surface of OSB was 60°C and on the interior surface of OSB was 58°C. A vertical temperature gradient was observed once at the OSB and continued through the entire wall. The range between the lowest and the highest surface temperature on both exterior and interior surfaces of OSB was approx. 10°C.

Temperature gradient that was observed on the surfaces of OSB continued to exterior and interior surface of gypsum board as well. This temperature gradient was approximately 3°C on the exterior surface of the gypsum board and 2°C on its interior surface.

3.3.2.3 Vapor pressure across wall 2

Figure 3.38 below shows the vapor pressure in the insulation cavity, air cavity and interior of the hut of this test specimen. Figure 3.39 shows the differential vapor pressure between the air cavity and insulation cavity, and between the insulation cavity and inside the hut.

The moisture contents of the wood stud gravimetric samples underwent the same trend that was observed for the gypsum board samples. Very little increase of moisture content (approximately 6 kg/m^3) was observed in these samples.

The low moisture content of the gypsum board and wood gravimetric samples was a result of the vapor open interior finish of paint which allowed drying of the moisture towards inside.

3.3.3 Test results of wall 3 (brick/XPS/VWC)

This wall was constructed of exterior brick veneer cladding and interior back wall with Extruded Polystyrene Insulation (XPS) exterior sheathing, instead of the OSB which was used for the other wall specimens, and gypsum board covered with VWC. The air cavity in this test was not vented. This test was performed for 20 days, from November 20, 2007 to December 10, 2007, including 11 days of cycling wetting and drying periods, and 9 days of drying. Appendix F presents the graphs plotted from the measured data from testing this assembly.

3.3.3.1 Environmental conditions

In this section, the environmental conditions of the inside and outside of the tested assemblies and the ambient conditions of the laboratory are reported (Figures 3.43 and 3.44). No data of the relative humidity and temperature inside the air cavity was recorded from day 2 to day 19. This was due to malfunctioning of the RH probe in the air cavity which was a result of a very high level of relative humidity at this location. At day 19, when the RH was low enough for the RH probe to perform correctly, the RH probe of the outside of the radiation box was placed inside the air cavity, and the condition in the air

The temperature in the air cavity was only recorded for the first and last 1.5 days of the test period. During the first 1.5 days of the test, temperature got as high as 47°C with a bracket of 26°C between the minimum and maximum temperatures. The relative humidity in the air cavity during this period reached a maximum of 100%, while it decreased to 65% by the end of the daily wetting period. The temperature level as well as its average value increased from the beginning to the end of the test period. During the last 1.5 days of the test period, the temperature reached 60°C, with a difference of 38°C between the minimum and maximum values. The relative humidity in the air cavity dropped by 50% by the end of the test period, reaching maximum of 50% and minimum of 19% during the last 1.5 days.

The temperature inside the insulation cavity varied with each test cycle. The difference between the lowest and highest temperatures in the insulation cavity was approximately 3°C during the cycling wetting and drying period of the experiment, which increased to approximately 4°C after the start of the drying phase. The relative humidity in the insulation cavity started with approximately 46% at the beginning of the experiment and kept increasing during the test period having cyclic pattern during each day. The relative humidity in the insulation cavity reached a maximum of 70% at the end of the wetting period, stayed at that level for 7 days and started to decrease during the last 2 days of the measurements, reaching 62% at the end of the test period.

gradient could be due to convection loop or air stratification in the insulation cavity. The moisture content of the top sample reaches a maximum of 9.6 kg/m^3, the middle specimen reaches a maximum of 6.5 kg/m^3 and the bottom specimen reaches a maximum of 4.4 kg/m^3 by the end of the test period. Although moisture accumulation occurs, the maximum values reached are much smaller than the one seen in wall 1.

The moisture contents of the wood stud gravimetric samples undergo the same trend in terms of the variation of moisture content that was observed for the gypsum board samples, with the top sample having the greatest increase of moisture content, and the middle and bottom sample having smaller increase. The moisture content of the top stud sample reaches a maximum of 121 kg/m^3, having a total increase of 30 kg/m^3, the middle sample reaches a maximum of 108 kg/m^3 with a total increase of 8.5 kg/m^3 and bottom sample reaches a maximum of 46 kg/m^3 with a total increase of 3.3 kg/m^3 by the end of the test period.

3.3.4 Test results of wall 4 (stucco/OSB/VWC)

This wall was constructed of exterior cement stucco cladding directly applied on the OSB of the backwall and with gypsum board on its interior covered with VWC. Thus, the stucco cladding and wood frame backwall for this specimen is incorporated into one assembly, with no air gap between the backwall and the cladding. This test was performed for 18 days, from May 12, 2008 to May 30, 2008, including 8 days of cycling wetting and drying periods, and 10 days of drying. Appendix G presents the graphs plotted from the measured data from testing this assembly.

wetting phase was terminated and drying phase was started. Maximum temperature on this surface was 59°C.

On the exterior surface of the gypsum board, surface temperature reached a maximum of 22°C during the first 14 days and dropped by 1°C during the last 4 days of the test. On the interior face of the gypsum board, the maximum temperature was approximately 18.5°C during the entire test period.

A vertical temperature gradient was observed on the interior surface of OSB to a small degree during the drying period of the test, which continued on the exterior and interior surfaces of gypsum board as well. This temperature gradient was approximately of 2°C on the interior surface of OSB, 2°C on the exterior and 1°C on the interior surfaces of the gypsum board.

3.3.4.3 Vapor pressure across wall 4

Figure 3.58 below shows the vapor pressure in the insulation cavity and interior of the hut of this test specimen. Figure 3.59 shows the differential vapor pressure between the insulation cavity and inside the hut.

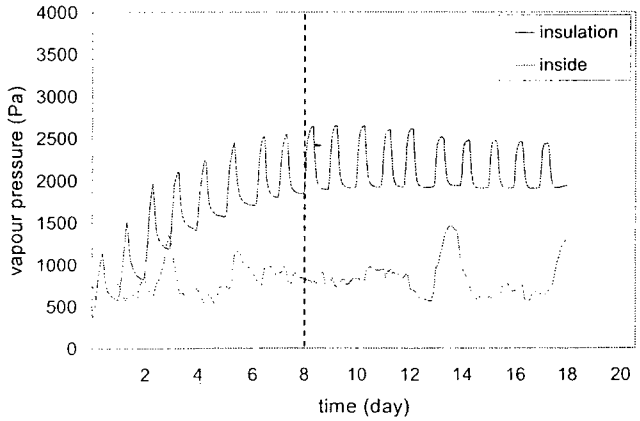

Fig. 3.58 Vapor pressure across wall 4

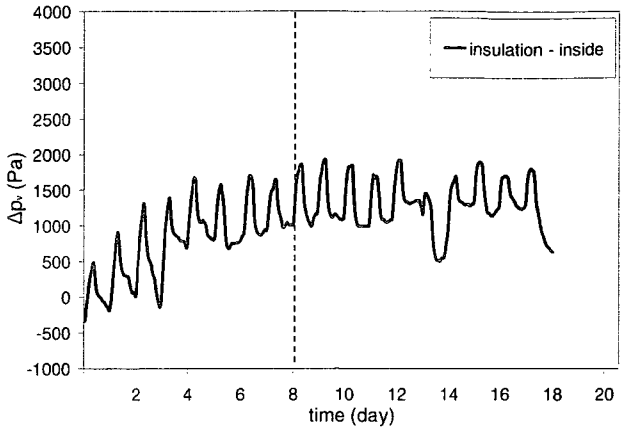

Fig. 3.59 Differential vapor pressure across wall 4

The vapor pressure in the insulation cavity varied during the daily test cycles reaching a maximum of 2643 Pa. The magnitude of the vapor pressure in the insulation cavity as well as its fluctuation stayed the same for 13 days after the end of the wetting period, after which it started to drop, reaching a maximum of approximately 2390 Pa by the end of the test period. The vapor pressure inside the test hut was approximately 850 Pa during the entire test period while peaking to a maximum of 1406 Pa at a point.

During the entire duration of the test, as shown on Figure 3.59, the vapor pressure in the insulation cavity was higher than inside the hut, although moisture drying towards inside was quite slow due to the presence of the vapor tight wall covering. Therefore, drying of the wall was mostly towards outside and it began only after the start of the drying phase at day 8. Comparing this test with the previous tests indicated a higher vapor pressure difference between the insulation cavity and interior of the hut for this test. This was due to the moisture in the stucco layer in direct contact with the backwall, as no air cavity was present. This moisture is driven inside the insulation cavity resulting in a high vapor pressure in the insulation, as confirmed by high relative humidity in the insulation cavity of 90% to 100%. Looking at the surface temperature of the interior side

of the OSB, we can see that this surface temperature is higher than the previous tests with the brick cladding and air cavity. Therefore the temperature gradient across the insulation cavity is higher in this test, resulting in a large vapor drive towards inside.

3.3.4.4 Moisture content variation results

Figure 3.60 shows the change of moisture content of the entire specimen in kg/m^2.

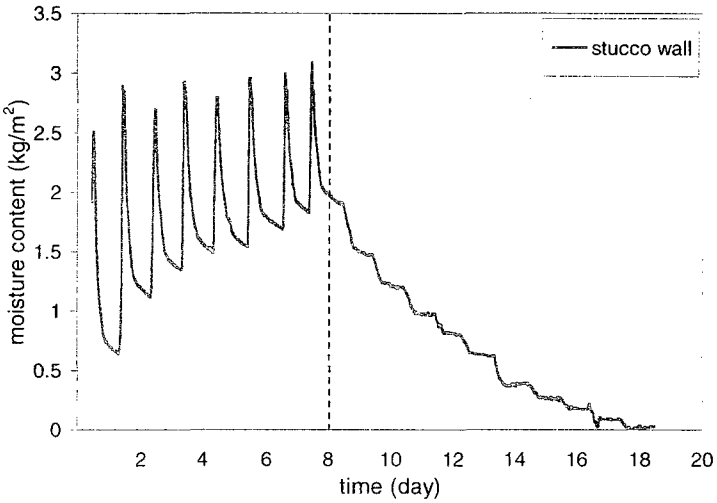

Fig. 3.60 Moisture content of wall 4

The moisture content of the entire wall increased to approximately 2.7 kg/m^2 during each wetting period and decreased with every radiation cycle, although less with each cycle as some moisture was accumulating in the backwall. The moisture content of the wall experiences a rapid decrease as soon as the drying period begins. The amount of moisture accumulated in this wall was higher than what was measured in the three previous specimens, as the moisture is accounted for both the stucco cladding and the backwall.

the end of the test period, moisture content of the bottom sample went back to its original amount while the moisture content of the top sample was 29 kg/m^3 (28 kg/m^3 above its initial moisture content) and the middle sample was 9.5 kg/m^3 (8 kg/m^3 above its initial moisture content).

The wood stud gravimetric samples very similar behavior. The maximum moisture content of the wood sample reached 46 kg/m^3 at day 14 of the experiment and stayed the same until the end of the test period. This moisture content was approx. 18 kg/m^3 higher than its initial moisture content.

The stucco gravimetric samples showed the same trend in terms of variation in moisture content that was observed for the entire wall, while being lower in magnitude. Daily variations of the moisture content of the stucco samples can be observed. The bottom sample reached higher maximum moisture content (approx 2.2 kg/m^2) than the top and middle one. The top and middle samples reached maximum moisture contents of 1.9 kg/m^2 and 1.8 kg/m^2 respectively. All samples started drying as soon as the wetting phase ended, with the top sample drying the most. The moisture content of the samples at the end of the test period was very close to their initial values, being 0.3 kg/m^2, 0.4 kg/m^2 and 0.5 kg/m^2 for the top, middle and bottom samples respectively. These amounts were approximately 0.1 kg/m^2, 0.2 kg/m^2 and 0.3 kg/m^2 above their initial moisture contents.

Regarding the moisture content of OSB, this test was the only test in which these measurements were possible. This was due to the higher level of moisture content of OSB in this test compared to the rest of the tests. The moisture content of the sheathing increased throughout the wetting period, and had a maximum amount by the end of this period while starting to decrease as soon as the drying period starts. Moisture content at

the middle of OSB was the greatest of all reaching a maximum of approximately 28%. The moisture content of the bottom of the OSB reached a maximum of 25%, while the top of the OSB reached a maximum of 23% being the lowest of all. This difference in moisture content at different locations of OSB and the top being the lowest could be due to uneven wetting of OSB due to uneven construction of the stucco cladding. However, the difference is within the error of the electronic probes.

3.3.5 Test results of Wall 5 (brick/VWC/vented)

This wall was constructed of exterior brick veneer cladding and interior back wall with OSB sheathing and gypsum board covered with VWC. Air movement in the air cavity was possible in this test as the brick cladding was vented at the top and bottom. Six vent holes in total (3 at the top and 3 at the bottom) were incorporated in the exterior brick cladding with a distance of 2 brick between vent holes. This test was performed for 20 days, from February 12, 2008 to March 2, 2008, including 11 days of cycling wetting and drying periods, and 9 days of drying. Appendix H presents the graphs plotted from the measured data from testing this assembly.

3.3.5.1 Environmental conditions

In this section, the environmental conditions on the inside and outside of the tested assemblies and the ambient conditions of the laboratory are reported (Figures 3.65 and 3.66). No relative humidity and temperature data were recorded on day 4 and parts of day 20 at the outside of the radiation box. This is due to malfunctioning of the RH probe during these days.

radiation only, reaching a maximum of 72°C. On the interior surface of the brick veneer, the maximum surface temperature increased by approximately 6°C after the wetting phase was terminated and the drying phase was started. Maximum temperature on this surface is 64°C.

A temperature gradient was observed on the exterior and interior surfaces of the brick cladding which was continued on the other inwards surfaces of the wall. A maximum difference of approximately 10°C between the top and bottom thermocouple can be seen on the exterior surface of the brick cladding, while this gap increases to approximately 15°C on its interior surface.

The surface temperature behavior observed on the first two surfaces (increase of the maximum surface temperature after start of the drying phase, as well as formation of the temperature gradient) is also seen on the exterior and interior surfaces of OSB as well. Maximum surface temperature on the exterior surface of OSB was 60°C and on the interior surface of OSB was 55°C. The formation of a temperature gradient from bottom to top was observed on both surfaces of OSB. The maximum difference between the maximum and minimum temperature was approximately 22°C on the exterior surfaces and approximately 15°C on the interior surface of OSB.

The vertical temperature gradient that was observed on the surfaces of brick cladding and OSB continued to the exterior and interior surfaces of gypsum board as well. This temperature gradient was between 4°C to 6°C on exterior surfaces of the gypsum board and approximately 2°C on its interior surface.

approximately 260 Pa by the end of the test period. The vapor pressure in the insulation cavity stayed quite constant during the entire test period (average 600 Pa), while also varying during each daily cycle. The vapor pressure inside the test hut was also quite constant having an average of approximately 400 Pa.

From Figure 3.71, it can be seen that the vapor pressure in the air cavity was higher than that of the insulation cavity for the first week of the test, during which moisture was driven to the insulation cavity, where accumulated in the gypsum board due to the presence of the wall covering. After 7 days, the vapor pressure of air cavity and insulation cavity reached almost the same level, allowing drying of the insulation cavity moisture towards outside. The vapor pressure of the insulation cavity was almost always higher than that of the interior of the hut during the entire test period, although the presence of the vapor tight wall covering on the interior led to an increase of the moisture content of the gypsum samples.

3.3.5.4 Moisture content variation results

Figure 3.72 below shows the change of moisture content of the brick cladding and back wall of this specimen in kg/m^3 and kg/m^2 respectively.

days after starting of the drying period), having a total increase of 9.6 kg/m^3, the middle sample reaches a maximum of 28 kg/m^3 with a total increase of 6 kg/m^3 and bottom sample reaches a maximum of 26 kg/m^3 with a total increase of 4.8 kg/m^3 by the end of the test period.

3.3.6 Visual inspection

After completion of each, the wall assemblies were disassembled to inspect the condition of the interior of the assembly and the individual elements visually. The observations conquered with the moisture level monitored. The condition of each tested wall that was inspected visually is described in Appendix I.

3.4 Comparative analysis

In this section, the test results of all wall assemblies are compared to one another. This includes comparison of: backwall moisture content in section 3.4.1, comparison of the brick wall moisture content in section 3.4.2, comparison of gypsum board and wood stud gravimetric sample moisture content in sections 3.4.3 and 3.4.4, comparison of the vapor pressure difference between the insulation cavity and inside, and vapor pressure difference between the air space and the insulation cavity in section 3.4.5.

3.4.1 Backwall moisture content comparison

Figure 3.75 shows the moisture content of the backwall of the four tested assemblies with exterior brick cladding.

Comparing the results of wall 1 with wall 2, i.e. with vapor tight VWC versus paint, clearly shows the effect of having a vapor open interior finish. We can see that, in

case of wall 2, very little moisture was absorbed by the backwall and this moisture dried out as soon as the drying phase started.

Comparing the moisture content of the backwall of wall 1 and wall 3 shows the effect of having OSB sheathing versus the more vapor tight XPS sheathing. Less moisture was accumulated in the backwall of the wall with XPS although the increase of the moisture content of the backwall continued even after the start of the drying period. This was not observed in wall 1 although the overall moisture accumulation was higher. This can be explained by the XPS sheathing in wall 3 not allow the drying of moisture out of the insulation cavity towards outside after the drying phase starts. In the case of the wall with OSB, drying of moisture towards outside starts after a couple of days into the drying period.

Comparing the results of wall 2 and wall 5 shows the effect of having a vented air cavity in minimizing moisture accumulation in the backwall. The moisture accumulation in the backwall of wall with vented air cavity is much less than that of the wall with sealed air cavity. Ventilation allows moisture that is driven in the air cavity from the wetted brick masonry to be removed from the air cavity before it is driven inside the backwall.

3.4.4 Wood stud gravimetric sample moisture content comparison

Figure 3.78 shows the moisture content of the wood stud gravimetric samples of all tested walls. These results provide complementary insights of the moisture conditions in the back wall and must be looked at together with the gypsum board results.

The overall patterns of moisture content variation in wall 1 was similar for the wood and gypsum board specimens, with a steady increase in moisture content during wetting, although the drying is much slower for the wood stud than for the gypsum board. For all other 4 walls, the patterns of MC variations for the wood and the gypsum board are similar. However, two main differences occur. The first difference in seen in wall 3, with XPS, where the moisture content of wood samples was similar to the one reached by wall 1, whereas the gypsum board moisture contents were much lower in wall 3 than in wall 1. This indicates that the moisture flow was regulated by the XPS in wall 3, more than by the VWC. SAS for the second difference, the top wood sample in wall 4 did not reach higher moisture content than the same sample of wall 1, whereas the other wood samples (middle and bottom of walls 1 and 3) had similar behavior. This difference is not explained yet. The wood studs in walls 2, with paint, and 5, with vented cladding, had constant moisture content through the walls, as also seen in the gypsum board samples.

- the interior finish plays a clear role in the accumulation of moisture in the interior gypsum for walls subject to important inwards vapor flows,
- the air space helps in reducing the magnitude of the inward vapor flow (brick versus stucco), but that the ventilation of the air space seems to be even more effective,
- even a vapor close sheathing does not stop sufficiently vapor flow to prevent moisture accumulation in the wood studs and the interior gypsum board,
- drying of the backwall occurs slowly due to the high inwards thermal gradient and in presence of a vapor tight interior finish, once the moisture source is stopped.

Conducting these experimental tests, it was observed that the large-scale tests almost constantly present variations in moisture content and temperature along the height of the specimens, with higher moisture content and temperature found at the top or at the top and middle of assemblies. This matter was investigated further in chapter 4. For this purpose, additional experimental studies were undertaken to observe the temperature and water vapor profiles in the insulated cavity of the wall. Also numerical studies were performed using the computational fluid dynamic software of Fluent. These numerical studies investigated the air movement patterns in the insulated cavity and the way it effects the temperature and water vapor profiles. The results of these studies will follow in the next chapter.

In the case of the specimen with stucco cladding, no clear temperature gradient was seen until the surface of gypsum board facing the exterior where the maximum temperature difference was approximately 2°C. This gradient continued to the inner face of the gypsum board with a maximum temperature difference of approximately 1 °C (Figure 4.2).

After verifying that no construction defect was present, i.e. that the gypsum board was installed tightly against the wood framing such that no gaps could let hot and humid air to be driven towards the top part of the framing, to enhance airtightness, the entire joint between the gypsum board and wood framing was sealed. Repeating the test showed no different in the previously observed temperature gradients. At this stage, two main scenarios were considered as possible causes of this temperature gradient:

1. A convection loop was occurring in the insulation cavity, which would carry warm and moist air towards the top section of the cavity where it was absorbed by the gypsum board.
2. Air and temperature stratification was occurring in the insulation cavity. This could be caused by the rise of hot and moist air in the cavity which had a lower density.

Thus, these two scenarios were further investigated by conducting experimental and numerical studies to observe heat and moisture pattern in the insulation cavity. This work is reported in this chapter. The experimental studies carried out to investigate the temperature and water vapor profiles are explained in sections 4.1 and 4.2. Section 4.3 includes a theoretical study of occurrence of convection loop. Sections 4.4 and 4.5 details

the numerical study undertaken to study the temperature and water vapor profiles. A conclusion of these studies will be made in section 4.6.

4.1 Experimental study of the temperature profile

The temperature profile in the insulation cavity was experimentally studied using a test setup similar to the one used for the studying of the solar-driven vapor transport with a higher number of monitored points.

4.1.1 Test procedure

For the purpose of this experimental study, the specimen with stucco cladding was used while increasing the number of thermocouples at various layers of the wall to 48, of which 21 thermocouples were positioned inside the insulation cavity. This array was required to obtain detailed temperature contours across the wall and especially in the insulation. The insulated cavity had a dense mesh of thermocouples. The thermocouples were held in place between layers of fiberglass insulation using in-tension fishing wire to ensure that their location were fixed. Figure 4.7 shows the installation process of the thermocouples in the insulation cavity and Figure 4.8 shows the exact locations of the thermocouples.

found possible that the position of the thermocouples in the insulation cavity might have slightly shifted during handling, and thus might not be at their intended location.

4.2 Experimental study of water vapor profile

Water vapor profile in the insulation cavity was also experimentally studied. For this purpose, a test setup similar to the one used for the study of the solar-driven vapor transport was utilized with a higher number of monitored points.

4.2.1 Test procedure

For the purpose of this study, the specimen with stucco cladding was also used. The specimen was exposed to air conditioned indoor condition on one side, and cyclic periods of wetting and drying, simulating rain and sun, on the other side. The stucco cladding was wetted to 50% capillary saturation at the beginning of each test cycle. This was done using a spray apparatus which was calibration to evenly wet the surface of the cladding. The specimen was then exposed to 8 hours of radiation followed by 16 hours of drying with no radiation. This process was repeated for 5 days, after which the spraying was stopped and the wall was only exposed to cyclic solar radiation for 4 more days.

To study the water vapor pattern through the wall in more detail, total of 10 relative humidity sensors were installed through the wall. Locations of the sensors were the same as the ones noted for the solar-driven vapor transport studies, as per Figure 3.17, although for this test, sensors were installed at three different heights (top, middle and bottom) rather than only at the centre. Thermocouples placement was the same as the previous tests as per Figure 3.17, at all interfaces and at three heights (top, middle, and bottom).

4.3 Theoretical study of occurrence of convection loop

In order to study the occurrence of convection in the insulation cavity theoretically, the porous Rayleigh number was calculated using the equation 2.7 given in chapter 2. The values of the parameters used for calculating this value are given in Table 4.1 below. The thickness of the insulation cavity is 0.089m and the temperature difference is 42°C.

The value of porous Rayleigh number calculated for our case is 1.94. This value is well below the critical porous Rayleigh number of 4 to 6 (Bankvall, 1972; Schneider, 1963; Kohonen et al., 1985) which is for low aspect ratios (1 to 10) and 20 for aspect ratio of 50. The aspect ratio in our study is approximately 27 for which the critical Ra_o is expected to be approximately 13. The low value of Ra_o, 1.94, being below the critical values does not mean that no convection loop is present in the insulation cavity, but it shows that the convection loop will not be strong enough to affect the thermal properties of the insulation material and result in convective heat loss. These results show that no major air movement is happening in the insulation cavity, therefore the air movement , which is quite low, most probably does not cause a vertical temperature gradient on the interfaces of the insulation cavity.

To verify the accuracy of the calculated value of Ra_o, parameters of studies by Kohonen et al. (1985), Bankvall (1972), and Okland (1998) were used to calculate Ra_o. The calculated Ra_o values are compared to what is reported by them.

Kohonen et al. (1985) had an insulation cavity of 0.3m wide, filled with insulation having an air permeability of 6.0E-9 m^2 (parallel to flow) and thermal conductivity of

0.034 W/mK. The temperature difference across the assembly was 40°C. They calculated Ra_o to be 5.2 while we calculated it to be 5.76.

Bankvall (1972) had an insulation cavity of 0.14m wide, with insulation material with air permeability of 1.1E-8 m^2 parallel to heat flow, and thermal conductivity of 0.0355 W/mK. The temperature difference across the assembly was 35°C. He calculated Ra_o to be 5.0 while our calculation showed it to be 3.73.

Okland (1998) had an insulation cavity of 0.3m and an insulation material with air permeability of 3.69E-9 m^2 parallel to heat flow and thermal conductivity of 0.035 W/mK. The temperature difference across his assembly varied between 23°C to 38°C. For the purpose of this study we use 38°C. His calculated Ra_o was 3.5 while ours was 3.27.

It can be noted that the value of Ra_o calculated by us using the parameters of the above studies is very close to what is reported in studies themselves. This shows the accuracy of the Ra_o we calculated for our own case.

4.4 Numerical study of temperature profile

In this section, the aim is to use modeling to understand better the causes of the temperature, and moisture in the next section, distributions that were measured. In order to do this, the computational fluid dynamic software of Fluent was used. This tool was chosen since it would allow a close study of the air movement in the wall assembly which would not possible to do with heat and moisture transport codes such as WUFI or HAMFEM. Section 4.4.1 explains the description of the mesh and the domain used for this study. Boundary conditions and modeling parameters are described in sections 4.4.2 and 4.4.3 respectively. A verification study is followed in section 4.4.4. Section 4.4.5

provides the achieved results and section 4.4.6 is a discussion on the gathered results. This study ends with section 4.4.7 which is a sensitivity study.

4.4.1 Mesh and domain

The mesh was produced using Gambit which is a software used in combination with Fluent. A 1.2 m x 2.4 m domain is using a structured pattern, to form 20352 cells. Figure 4.15 shows the top half of the grid and Figure 4.16 is a close up of the top section of the grid showing the mesh in detail. The domain consists of a 0.01905m exterior stucco layer and 0.009 m OSB layer, which are set as solid material. A 0.089 m insulation cavity is set to contain air which is filled with insulation material with porosity of 0.994. The last layer is a 0.0125 m gypsum board. Sections of wood are placed at the top and bottom of the wall as solid materials representing the wood framing. Table 4.1 below shows the properties of the materials used for this domain.

Table 4.1 *Properties of material used for numerical study*

Material	Density, ρ (kg/m^3)	Specific heat, c_p (J/kg.K)	Thermal conductivity, λ (W/m.K)
Air	1.2[1]	1006.43[1]	0.025[1]
Stucco	1900[2]	850[2]	0.8[2]
Wood (spruce)	455[2]	1500[2]	0.23[2]
Gypsum board	850[2]	850[2]	0.2[2]
Insulation	13[3]		0.042[3]
OSB	553[2]	1700[2]	0.12[2]

(1) Fluent's data base
(2) WUFI's data base
(3) material property (provided by the manufacturer)

The Dynamic viscosity of air is 1.789e-5 kg/m.s, and its thermal expansion coefficient is 0.003165 1/K. The air permeability value of the fiberglass insulation is based on measurements by Oak Ridge National Laboratories (Stovall, 2008). This value

Nield and Bejan (1992) mention that "the flow in porous material is not turbulent since the irregularities are calmed down by the solid material and cannot be similar to that in pure fluid".

The solver was a 2D pressure based solver, with absolute velocity formulation, Green-Gauss-cell based gradient option, implicit formulation and steady time. Energy equations are activated and a first-order upwind scheme is used as the discretization scheme for energy and momentum. A body force weighted scheme is used for pressure discretization.

4.4.4 Verification study

A study to verify the accuracy of the numerical model created for this study was performed. For this purpose, studies by Kohonen et al. (1985) and Okland (1998) were used. It should be noted that in our CFD study, the width of the insulation was fixed at 0.089m and it was not modified for this validation study.

Kohonen et al. (1985) conducted a numerical study using CCC2D computer code on a structure 2.2m high and 0.3m wide. The temperature difference across the assembly was 40°C and the insulation material had a density of 17 kg/m^3 and air permeability of 3.2E-9 m^2 (perpendicular to flow), and 6.0E-9 m^2 (parallel to flow). In their study, the flow field inside the cavity showed a convection loop with maximum velocity magnitude of 2.5E-4 m/s. Using these parameters, our CFD study showed the maximum velocity to be 2.29E-4 m/s, very close to the calculated value by Kohonen et al. (1985).

Another study used for the model verification is the one by Okland (1998). Using LATENITE modeling software, he studied air flow in an insulation cavity with dimensions of 1.2m x 2.4m (L x H) and 0.3m thick filled with fiberglass insulation batts

having a density of 18 kg/m^3 and air permeability of 1.86E-9 m^2 (perpendicular direction), and 3.69E-9 m^2 (parallel direction). The warm surface temperature was 23°C and cold surface was 0°C for first 15 days, and -15°C for next 40 days. His study showed a convection loop in the insulation cavity where the maximum velocity was 1.6E-4 m/s. Using these parameters, our CFD study showed the maximum velocity of 1.41E-4 m/s, quite close to the calculations by Okland (1998).

4.4.5 Results

The results of the simulations are presented in this section. First the velocity profile in the insulation cavity is studied. Figures 4.17 and 4.18 show the velocity vectors in the insulation cavity, in the entire wall and at the top section of the wall, respectively. It can be seen that the maximum velocity achieved in the insulation cavity is 3.21E-4 m/s which is very low. Further, the temperature profile through the entire wall is studied. Figures 4.19 and 4.20 show the temperature profile in the entire wall and the top portion of the wall, respectively. In these figures, temperature is shown in °C. Temperature profile across the wall is quite uniform and little impact air movement can be observed. Further, the temperature profile on surface of the gypsum board facing outside and surface of OSB farcing inside is studied in Figure 4.21. The three vertical lines represent the location of the thermocouples used for the experimental tests.

bottom of the wall. Therefore the modeling results show that no significant convection loop is created in the insulation cavity which is strong enough to cause the temperature gradient which was observed during the experiments.

4.4.7 Sensitivity studies

To ensure validity of the CFD results, a sensitivity study was undertaken. First, a simulation was conducted to study the air movement in the insulation cavity, without the presence of insulation and only with air in the cavity. The viscous model used for this study was a turbulent K-Epsilon model since air flow in the cavity without the porous insulation in it could be turbulent. Results show an increase in the magnitude of the maximum velocity by a factor of 536 (53482%). For this case, a maximum temperature difference of 2°C is observed on the interior surface of the gypsum board.

Further, the effect of variation of the air permeability of the insulation was studied. Increasing the permeability by factor of 10 and 100 shows an increase of the maximum velocity by factors of 10.4 and 109.3 respectively (940% and 10803%). Decreasing the permeability by factors of 0.1 and 0.01 shows a decrease of the maximum velocity by factors of 0.1 and 0.01 respectively (90% and 99%). In all these cases with insulation, the maximum velocity is still not high enough to result in a significant air circulation that would cause a temperature gradient along the face of the gypsum board.

A grid sensitivity study was performed by increasing the number of cells. By doubling the number of cells on each face and increasing the total number of cells to 41808 (by a factor of 2.05), no change in the magnitude of the maximum velocity is observed. Increasing the number of cells by a factor of 4 also shows no change in the maximum velocity magnitude.

4.5 Numerical study of water vapor profile

In this section, details and results of the numerical study of water vapor profile in the insulation cavity, using Fluent, are presented. The mesh and domain used for this study is the same as the previous study of temperature profile. Boundary conditions and modeling parameters are described in sections 4.5.1 and 4.5.2, respectively. Section 4.5.3 presents the achieved results. The results are analyzed in section 4.5.4, followed by a discussion in section 4.5.5. This study ends with a parametric investigation of moisture gradient in the insulation cavity in section 4.5.6.

4.5.1 Boundary conditions

Since mass flow through solid material cannot be supported by Fluent, the actual case to reproduce the experimental conditions could not be reproduced. For the purpose of this study, the boundary conditions were chosen as such to produce similar conditions inside the insulation cavity to the ones achieved from the experimental results. Air flow and moisture flow was then studies in such a cavity.

The modeling was done as a steady state case. The exterior (warm side) surface temperature and water vapor mass fraction were 50°C and 0.0405 kg/kg, resulting in relative humidity of 50% on this boundary. On the interior side, temperature was set to 18°C and water vapor mass fraction was set to 0.0038 kg/kg, resulting in relative humidity of 30% on this face. The top and bottom boundaries of the domain were set as adiabatic.

4.5.2 Modeling parameters

The viscous model used for this simulation was the laminar model. Also to account for water vapor in the air, species model was used with the mixture being composed of water vapor and air. The density of the mixture was chosen as incompressible-ideal-gas and it thermal conductivity as ideal-gas-mixing-law.

The solver was a 2D pressure based solver, with absolute velocity formulation, Green-Gauss-cell based gradient option, implicit formulation and steady time. Energy equations are activated and a second-order upwind scheme is used as the discretization scheme for energy, momentum and H2O. A body force weighted scheme is used for pressure discretization.

4.5.3 Results

Initially, this study was performed using an insulation having the same air permeability as the one used in our experiments, i.e. 8e-9 m^2. Temperature profile and velocity vectors in the insulation cavity are shown in Figures 4.22 to 4.24. A linear temperature profile can be seen across the wall having no signs of a vertical gradient. Studying air movement in the insulation cavity showed a circular movement pattern although the maximum velocity magnitude was very low (3.57e-4 m/s) which did not result in any significant air movement. Vapor pressure profile in the insulation cavity is shown in Figure 4.25. Having a linear profile across the wall, no vapor pressure gradient can be observed.

with higher air permeability, vertical temperature and vapor pressure gradients were observed.

Occurrence of the vertical temperature gradient in the insulation cavity can have two possible causes. Observing the occurrence of temperature gradient by increasing the air permeability of the insulation and therefore the air velocity in the insulation cavity shows that there can be a relation between the two. In the case with higher air permeable insulation, circular air movement in the insulation cavity moves the air with higher temperature at the left wall of the cavity, upwards. On the other side of the insulation cavity, cooler air is moved downwards due to this air circulation. This phenomenon can be a cause of the vertical temperature gradient that can be seen in Figure 4.28.

This phenomenon, being the increase of the magnitude of the air velocity by increase of the air permeability of insulation, was not observed in the results of the numerical study performed in the previous section to study temperature profile in the insulation cavity. In that case, the insulation cavity was filled with only dry air and no water vapor presence was considered. Adding water vapor to the air changes the density of the mixture, making it lighter. This could be the cause of the difference in the results achieved from these two studies.

Another cause of this temperature gradient can be upwards movement of air with higher temperature due to its lower density. This is known as air stratification.

Further, the occurrence of vapor pressure gradient in the insulation cavity was studied. For the purpose of comparison with the experimental results, vapor pressure values were studied on a vertical plane located 1cm inside the insulation cavity from the cold wall. This was the location of the relative humidity probes installed on the exterior

face of gypsum board in the experimental set up. Figure 4.30 shows the vapor pressure along this axis. The two vertical lines represent the location of the relative humidity probes installed in the experimental set up. Vapor pressure was approximately 1800 Pa at the top (30 cm from the top of the wall), and 1040 Pa at the bottom (30cm from the bottom up the wall) on this axis. This resulted in a vapor pressure gradient with a difference of 760 Pa from the bottom to the top of the wall. This vertical vapor pressure gradient is believed to be due to upwards movement of air and water vapor mixture which has a lower density than dry air. These results are similar to the experimental results where a difference of approximately 660 Pa was observed from the bottom to the top of the wall at this location.

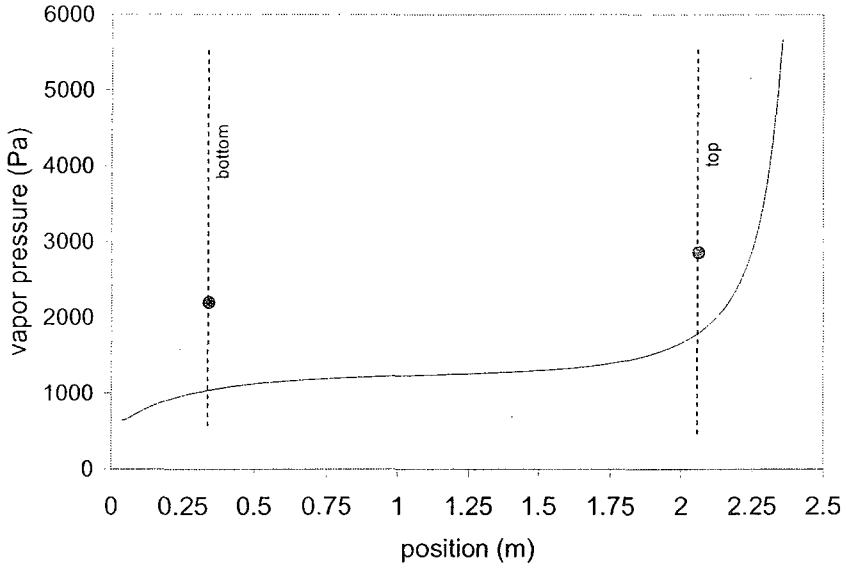

Fig. 4.30 Vapor pressure in the insulation cavity along a vertical axis 1cm into the insulation from the cold side

4.5.5 Discussion

Numerical study of water vapor profile in the insulation cavity using the air permeability of the insulation which was used in the experiments, showed no sign of a vertical vapor pressure gradient in the insulation cavity which was observed during the

experiments. By increasing the permeability of the insulation by a factor of 100, signs of air movement were observed as well as vertical temperature and vapor pressure gradients. Occurrence of significant air movements in the insulation cavity with higher air permeable insulation was not observed in the previous numerical studies where air was considered to be dry with no moisture added to it. Addition moisture to air makes it lighter which can affect its movement pattern in the insulation cavity. Therefore the present case, with air and water vapor mixture, is a better representation of our case.

Thus, the occurrence of the water vapor stratification in the insulation cavity is believed to be due to lower density of moist air and its upwards movement in the cavity. This was noted in the results achieved from the numerical studies, although only when insulation with higher air permeability was used.

Regarding the air permeability of insulation, since fiberglass insulation is quite light, its air permeability is installation dependent and it is possible and it was stretched or compressed at locations during installation which caused changes in its air permeability. Therefore it is possible that the insulation material which was used in the experimental tests had higher air permeability than what was originally assumed and used for the numerical studies.

4.5.6 Moisture gradient parametric investigation

Through a series of systematic numerical studies, effect of change of a number of parameters on the vapor pressure inside the insulation cavity was investigated. The location at which the vapor pressure profile was studied was 1cm inside the insulation cavity from the cold side (gypsum board side). This location was chosen since it corresponds to the location of the relative humidity/temperature probes installed in our

specimen during the experimental study. The investigated parameters were: exterior surface relative humidity and temperature, and interior surface relative humidity and temperature. For the purpose of this study, vapor pressure was observed at two different locations along the height of the wall, which correspond to the heights at which the relative humidity/temperature probes were installed during the experimental tests. These locations were 30cm from the bottom of the wall, and 30 cm from the top of the wall.

The studied range of these parameters for outside conditions were: 50°C to 60°C for outside temperature, 40% to 60% for outside relative humidity. Initially, effect of changing outside conditions on vapor pressure gradient in the insulation cavity was studied:

- By increasing the outside surface temperature, higher vapor pressure levels as well as larger vapor pressure gradient from bottom to top of the wall was observed. It was noted that this effect was even larger when outside surface also had a higher initial relative humidity.
- Increasing outside relative humidity level only, keeping outside temperature consistent, also resulted in larger vapor pressure gradient. This effect was larger when outside temperature was higher.
- Studying the effect of exterior conditions on the vapor pressure in the insulation cavity showed that increasing exterior temperature has greater influence on vapor pressure gradient than increasing outside relative humidity.

The studied range of these parameters for inside conditions were: 13°C to 18°C for inside temperature and 10% to 30% for inside relative humidity. Effect of changing interior conditions on vapor pressure gradient in the insulation cavity was studied:

- It was noted that lowering the interior surface temperature resulted in higher vapor pressure gradient inside the cavity. Vapor pressure gradient was slightly larger when this low interior temperature was accompanied by higher interior relative humidity levels.
- Decreasing interior relative humidity levels, while keeping inside temperature the same, resulted in an increase in vapor pressure gradient level. This effect is more when inside temperature was higher.
- Studying the effect of interior conditions on the vapor pressure in the insulation cavity showed that decreasing interior temperature has larger influence on vapor pressure gradient than decreasing interior relative humidity.

This parametric study showed how changing the interior and exterior boundary conditions can affect the vapor pressure conditions inside the insulation cavity. Since vapor pressure does not have a linear relationship with temperature and relative humidity, one cannot produce one set of data for vapor pressure gradient applicable to all cases.

4.6 Conclusion of temperature and water vapor profile studies

Numerical studies of air movement in the insulation cavity, using dry air as the medium in the cavity, showed no significant air movement in the insulation cavity and no temperature gradient on the interfaces of gypsum board. In this case, increasing the air permeability of the insulation material or changing outside and inside boundary

conditions did not affect the air flow pattern and temperature profile in the insulation cavity.

Adding moisture to the air in the insulation cavity, which is a closer representation of our experimental conditions, resulted in different air flow patterns. This is due to variation of properties of air when mixed with moisture. Moisture air has lower density than dry air and will behave differently when exposed to temperature and vapor pressure gradient. In this case, no significant air movement was observed when modeling with an insulation material having low air permeability similar to what was used in our experiments. However, increasing the air permeability of the insulation material resulted in higher air velocity magnitude in the insulation cavity which was accompanied by a vertical temperature gradient.

Therefore the numerical studies showed formation of a vertical temperature gradient on the exterior surface of gypsum board, although only for a case with high air permeable insulation material. This vertical temperature gradient can be either due to convective air movement in the insulation cavity caused by upward movement of warm air on the left wall and downwards movement of cold air on the right wall, or can be due to air stratification which is upwards movement of higher temperature air with lower density. It is also possible that the temperature gradient is a result of a combination of both these two effects. The exact cause of the air movement and consequent temperature gradient is unknown at this point and requires further numerical studies. Also further verification of the air permeability of the insulation material used in the experimental studies is necessary. This is in order to understand the lack of a significant air movement in the insulation cavity using the air permeability value of the actual insulation material.

The numerical studies also showed water vapor stratification in the insulation cavity and a vapor pressure gradient on an axis representing the exterior surface of gypsum board, although these results were only observed with modeling was done using a low air permeable insulation.

Therefore both temperature and water vapor gradients on the exterior surface of gypsum board were observed though the numerical studies, although these were only seen when the air permeability of insulation was high.

5 Guidelines derived from the research program

This section transfers the knowledge acquired though this research study to designers and practitioners and recommend strategies to improve the overall design and performance of the building.

In situation where the cladding of a wall assembly, which is wet either by rain or moisture accumulation from winter, is exposed to high outdoor temperatures, a high vapor pressure develops on the exterior side. This high outside vapor pressure causes a vapor pressure gradient from outside to inside. The vapor pressure gradient becomes even larger when accompanied by low vapor pressure on the interior side caused by air conditioning. This vapor pressure gradient causes inwards flow of water vapor though the assembly.

If the building envelope is vapor open, this moisture can easily flow though the wall without damaging any of the interior wall elements, although this is not always the case. The problem rises when the flow is restricted by a vapor tight layer. Water vapor then accumulates behind this vapor tight layer, gets absorbed be porous materials in contact with it, and over long term, damages these materials or cause mold and fungi on the wet surfaces.

5.1 Placement of the interior vapor tight layer

In areas with cold climate, this restriction of vapor flow is usually caused by a vapor tight membrane, either a polyethylene sheet or a vapor tight wall covering material,

which is placed on the warm side of the insulation (interior). The original purpose of this layer is to restrict outwards flow of water vapor during cold seasons and eliminate condensation. Not much attention has been paid into how this layer would influence the performance of the wall in warm seasons.

In area with hot and humid climate, restriction of inwards vapor flow is usually due to a vapor tight vinyl wall covering place on the interior of the assembly. Being a common decorative practice in many areas, its negative effects on the performance of the wall is rarely taken into account.

In order to eliminate the problems associated with inward vapor flow, water vapor that is present within envelope has to be permitted to exit.

In hot and humid climate areas, this can be done by using a vapor open interior finish such as paint. Water vapor permeability of a layer of acrylic paint is much higher than the water vapor permeability of vinyl wall covering. This design strategy allow free passage of inwards vapor flow though the assembly without causing any damage to the interior wall elements.

In cold climate areas, since a vapor tight interior layer is required to avoid winter condensation, solving the problem is not as easy. One strategy is using a humidity controlled vapor barrier instead of a low permeability polyethylene (Kunzel, 1999). This material gets highly permeable when exposed to high relative humidity levels in summer, while it performs like a good vapor barrier during winter.

Another strategy for cold climate areas is using a low-perm interior vapor barrier. In this case, the designer has to ensure that the permeability level of this material is high enough to avoid winter condensation and moisture accumulation.

A third strategy for cold climate area is eliminating water vapor entry into the assembly at the first place. This strategy will be explained in the next section in more detail.

5.2 Placement of the exterior vapor tight layer

Another strategy to eliminate problems associated with inward vapor flow is preventing such a flow at the first place. This can be done by installing a vapor tight layer on the exterior side of the wall assembly. This can be either a vapor tight exterior sheathing, or a vapor tight membrane installed over the sheathing.

If using a vapor tight exterior sheathing, care has to be taken into choosing an appropriate one. Water vapor transport properties of some materials used as exterior sheathing can be affected when exposed to high levels of relative humidity and it might not be as effective in eliminating inwards water vapor flow any longer.

When using this strategy, care has to be taken if the assembly is located in a cold climate area where the interior surface is also treated with a vapor tight material. Having two layers of vapor tight material on two sides of the wall cavity can be problematic. It is possible that water vapor passes the exterior vapor tight layers, through openings caused by damages or bad installation, and leak into the wall cavity. Since a vapor tight layer also exists on the other side of the cavity (the interior side), this entered moisture can be trapped in the wall cavity and damage the internal elements. This phenomenon can also happen during cold season and lead to the same problem when outwards vapor flow is occurring.

Therefore in cold climate areas, if a vapor tight exterior sheathing is used, it is suggested that the interior vapor tight membrane be eliminated. In order to solve the problem of winter condensation in this case, all the insulation material can be moved to the exterior side of this exterior vapor tight sheathing. This sheathing can even be the insulation material itself. Doing this, condensation plane moves further out and the vapor tight exterior sheathing can also act as the vapor barrier in cold seasons.

5.3 Incorporation of a ventilated air cavity behind cladding

Providing a ventilated air cavity between the cladding and the back wall is another method to eliminate the risks associated with inward vapor flows. The air cavity acts as a pressure equalizer by removing the water vapor that is driven inside cavity, and is accumulated behind the sheathing, to outside. This lowers the vapor pressure difference across the assembly and as a result, less moisture is driven towards inside. Size of this air cavity, as well as rate of ventilation, are also defining factors in its effectiveness which were not studied in this thesis.

5.4 Conclusion

It is found that nowadays designers do not have enough time to study all aspects of any specific building assembly, although they are open to improve their design and assemblies by integrating new achieved knowledge. Based on the results of the experimental studies which were presented in the previous chapter, this chapter provided some guidelines for designers. These guidelines are only for the types of wall assembly studied and tested as part of this thesis, being a wood framed assembly, filled with

insulating material, and with interior and exterior sheathings and an exterior porous cladding. The principles of these guidelines can be applied to walls with different construction, but care should be given then.

6 Conclusions

This thesis has presented an investigation of inwards moisture flow in wall assemblies exposed to cyclic rain and sun periods. The work demonstrates the importance of performing such a study using a systematic approach.

In this thesis, the hygrothermal performance of large-scale wall assembly specimens exposed to inwards moisture flow was studied experimentally. The experimental set-up consisted of: two weighing apparatuses to monitor the change of mass of the cladding and backwall parts of wall specimens, a spraying array, a radiation array, and a test hut to provide controlled interior conditions. Five insulated wood-framed walls were monitored. Four walls were brick cladded: with backwall with vinyl wall covering as interior finish, with backwall with paint as interior finish, with backwall with vinyl wall covering as interior finish and with extruded polystyrene instead of OSB as the sheathing, with backwall with vinyl wall covering as interior finish and air movement in the air space. One wall was with stucco as the exterior cladding material, no air space and a back wall finished with vinyl wall covering. The walls and the environment were equipped for electronic monitoring, complemented with manual weighing of gravimetric samples.

The results of the experimental part of this study demonstrated that:

- the vapor permeability of the interior finish plays a clear role in the occurrence of accumulation of moisture in the interior gypsum board for walls subjected to important inwards vapor flows,

- the air space helps in reducing the magnitude of the inward vapor flow (brick versus stucco), but that the ventilation of the air space seems to be even more effective,
- even a vapor close sheathing does not stop sufficiently inwards vapor flow to prevent moisture accumulation in the wood studs and the interior gypsum board,
- drying of the backwall occurs slowly due to the high inwards thermal gradient and, in presence of a vapor tight interior finish, occurs only once the moisture source is stopped.

Conducting these experimental tests, it was observed that the large-scale tests almost constantly present variations in moisture content and temperature along the height of the specimens, with higher moisture content and temperature found at the top or at the top and middle of assemblies. This matter was investigated further through additional experimental and numerical studies using computational fluid dynamic software of Fluent. These studies showed that:

- while experimental studies showed a vertical temperature and moisture content gradient on the gypsum board/ insulation interface, numerical studies, using low air permeable insulation material such as what was used in the experimental tests, did not show this. In the numerical studies, no significant air movement in the insulation cavity and therefore no temperature and moisture variation along the height of the wall were observed,
- Increasing the air permeability of the insulation material for the numerical studies showed signs of air movement in the insulation cavity when the air in the cavity

was mixed with moisture. The results of this modeling also showed variations in moisture content and temperature along the height of the wall.

6.1 Contributions of the research

This thesis aimed to study the occurrence of solar-driven vapor transport in wall assemblies in a very systematic approach. This section points how this was done by indicating the contribution of this work:

- Implementation of a test set-up to produce a unique set of data on inwards vapor flow in large-scale wall assemblies. Five assemblies were tested with various test durations. The collected data includes temperature, relative humidity and moisture content.
- A comparative analysis of the influence of various parameters on the inward vapor flow behavior of wall assemblies. These parameters were water vapor permeance of the interior finish and the exterior sheathing, presence of a ventilated air cavity, and porosity of the exterior cladding material.
- Understanding the behavior of individual wall elements, i.e. gypsum board and wood stud, exposed to inwards vapor flow. This was achieved by periodic weighing of the gravimetric samples.
- Discovering a vertical temperature and moisture gradient in the insulation cavity of the tested specimens which resulted in elevated moisture content levels at top sections of their interior elements.

The contributions of this research work through the numerical studies are:

- Highlighting temperature and moisture stratification in the insulation cavity of conventional wood frame wall assemblies when a high air permeable insulation is used. Numerical studies using computational fluid dynamic software of Fluent showed that when temperature and relative humidity gradient exists across the wall, a vertical temperature and vapor pressure gradient occurs in the insulation cavity. This phenomenon is more pronounced when the air permeability of the insulation material in the cavity is high.

6.2 Recommendations for future work

Although significant steps were achieved through this research project, some questions still remain that require further investigation. These are:

- studying the transport properties of various materials used in construction of a wall, at high temperatures and moisture contents. Transport properties of materials such as the interior finishes, weather resistive barriers, the exterior sheathings (OSB or XPS), or even the exterior cladding can change significantly as temperature rises or their moisture content increases. A wall assembly could be designed to perform better and be more durable if the temperature influence on its properties could be considered.
- quantification of ventilation rate in the air cavity. The test results in this study, as well as previous studies, have shown the effect of the ventilation of the air space in reducing the amount of inward vapor flow by removing moisture out of the building envelope. The level of this effect is related to the rate of the ventilation. Therefore in order to utilize this method more effectively, it is necessary to

understand and quantify the ventilation rate in the air space under exposure to natural conditions.

- further numerical modeling of air and moisture flow in the insulation cavity exposed to inwards vapor flow using a heat, air and moisture transport code. Since no vapor flux can be specified on the boundary conditions in Fluent, the exact experimental conditions cannot be simulated using this software.
- quantification of the air permeability of insulation material used in the experiments. This is in order to ensure the air permeability values used in numerical studies corresponds to what was used in the experiments and provide a better means of comparison between the results of the two studies.

References

Andersen, N.E. 1987. Summer condensation in an unheated building, Proceeding of Symposium and Day of Building Physics, Lund University.

ASHRAE. 2001. Handbook of Fundamentals, ASHRAE, Atlanta.

ASTM. 1998. Application of Portland Cement-Based Plaster. Standard C926-98a, American Society for Testing and Materials, Philadelphia.

ASTM. 1999. Installation of Lathing and Furring to Receive Interior and Exterior Portland Cement-Based Plaster. Standard C 1063-99, American Society for Testing and Materials, Philadelphia.

Bankvall, C.G. 1972. Natural convective heat transfer in insulated structures, Report 38, Division of Building Technology, Lund Institute of Technology, Lund, Sweden.

Carmeliet, J., Karagiozis, A., Derome, D. 2007. Cyclic temperature gradient driven moisture transport in walls with wetted masonry cladding, Part of the project "Nature, Significance and Control of Solar-Driven Diffusion in Wall Systems" 1235 RTP, Proceedings of Thermal performance of the exterior envelopes of whole buildings X, DOE ORNL, ASHRAE, Clearwater Beach FL.

Ciucasu C., Gilles J., Montoya E., Arquis E. 2005. Convection phenomena in loose-fill attics, Proceedings of the 7th Symposium Building Physics in the Nordic Countries, Reykjavík: Icelandic Building Research Institute and KTH - Building Technology.

Derome, D., Saneinejad, S., Carmeliet, J., Karagiozis, A. 2008. Comparison of small- and large-scale wall assembly specimens exposed to similar experimental conditions. Nordic Building Physics Symposium, Copenhagen.

Dyrbol, S., Svendsen, S., Elmroth, A.2002. Experimental investigation of the effect of natural convection on heat transfer in mineral wool, Journal of Thermal Envelope and Building Science, Vol. 26, No. 2, pp. 153-164.

Edelstein, J. 2007. Solar-driven vapor transport in lightweight walls in a hot and humid climate, M.A.Sc. (Building), CBS, DBCE, Concordia University, Supervisor: D. Derome.

E.I. du Pont de Nemours and Company, http://www2.dupont.com/ Tyvek_Construction /en_US /assets/downloads/K-05031_HW_Prod_Prop.pdf (2006)

Fluent 6.1 user's guide. February 2003

Hubbs, B., Hircock, M.2002. Building envelope performance monitoring.

Kan, V. 2002. Controlling sun eriven moisture: a laboratory investigation, Masters Thesis, Department of Civil Engineering, University of Toronto, Canada.

Karagiozis, A., Salonvaara, M. 2001. Hygrothermal system-performance of a whole building, Building and Environment Vol. 36, Issue 6, pp. 779-787.

Kohonen, R., Kokko, E., Ojanen, T. and Virtanen, M. 1985. Thermal effects of air flow in building structures, Technical Research Centre of Finland, Research Reports 367, Espoo, Finland.

Kumaran, M.K., Lackey, J.C., Normandin, N., van Reenen, D. 2006. Vapor permeances, air permeances, and water absorption coefficients of building membranes, Journal of Testing and Evaluation, pp. 241-245.

Kunzel, H.M. 1999. Flexible vapor control solves moisture problems of building assemblies – smart retarder to replace the conventional PE-Film, Journal of Thermal Envelope and Building Science, Vol. 23, pp. 95 – 102.

Kunzel, H.M. 2005. Adapted vapor control for durable building enclosures, 10DBMC International Conference On Durability of Building Materials and Components, Lyon, France.

Langlais, C., Arquis, E., McCaa, D.J. 1990. A theoretical and experimental study of convective effects in loose-fill thermal insulation, ASTM STP 1030, pp. 290-318.

Lawton, M., Brown, W. 2003. Considering the use of polyethylene vapor barriers in temperate climates, Proceeding of the Ninth Building Science and Technology Conference, Vancouver, Canada.

Le Breton, P., Caltagirone, J. P., Arquis, E. 1991. Natural convection in a square cavity with thin porous layers on its vertical walls, Journal of Heat Transfer, Vol. 113, No. 4, pp.892-898.

Pressnail K., Timusk J., Kan L., Doug B., Kan V. 2003. In search of a wall for all seasons: controlling sun-driven moisture, Proceeding of the Ninth Conference on Building Science and Technology, Vancouver, Canada.

Roels, S., Janssen, H., Carmeliet, J., de Wit, M. 2006. Hygric buffering capacities of encoated and coated gypsum board, 3rd International Building Physics Conference, Montreal, Canada, pp.27-32.

Sandin, K. 1993. Moisture conditions in cavity walls with wooden framework, Building Research and Inf., Vol 12, No. 4.

Schneider, K.J. 1963. Investigation of the influence of free thermal convection on heat transfer through granular material, Proceeding of the 11th Int Cong of Refrigeration, Paper No. 11-4, pp. 247-253.

Shankar, V., Hagentoft, C.E. 2000. A numerical study of effect of natural convection on thermal properties of horizontal oriented porous insulation, Journal of Thermal Envelope & Building Science, Vol. 24, No. 2, pp.155-167.

Sherwood, G.E. 1985. Condensation potential in high thermal performance walls-hot, humid summer climate, Res. Pap. RPL 455. Madison, WI:US Department of Agriculture, Forest Service, Forest Products Laboratory.

Silberstein, A., Langlais, C., Arquis, E. 1990. Natural convection in light fibrous insulating materials with permeable interfaces: onset criteria and its effect on the Thermal performances of the product, Journal of Building Physics, Vol. 14, No. 1, pp. 22-42.

Southern, J.R. 1986. Summer condensation within dry lined solid walls. Building Services Engineering Research & Technology, Vol. 7, Issue 3, pp. 101-106.

Stovall, T. 2008. Personal communication.

Straube, J.F., Burnett, E.F.P. 1998. Drainage, ventilation drying, and enclosure performance, Thermal Performance of the Exterior Envelopes of Buildings VII, Clear Water Beach, Florida, pp. 189-198.

Straube, J.F., Burnett, E.F.P. 1995. Moisture movement in building enclosure wall systems, Proceeding of Thermal Performance of the Exterior Envelopes of Buildings VI. Atlanta, Geo., American Society of Heating, Refrigeration, and Air-Conditioning Engineers, Inc.

TenWolde, A., Mei, H.T. 1985. Moisture movement in walls in a warm humid climate, Proceeding of ASHRAE/DOE/BTECC Thermal Performance of the Exterior Envelops of Buildings III, pp. 570-582. Atlanta: American Society of Heating, Refrigeration, and Air-Conditioning Engineers, Inc.

Wahlgren, P. 2007. Overview and literature survey of natural and forced convection in attic insulation, Journal of Building Physics, Vol. 30, No. 4, pp.351-370.

Wahlgren, P. 2002. Measurements and simulations of natural and forced convection in loose-fill attic insulation, Journal of Thermal Envelope and Building Science, Vol. 26, No. 1, pp. 93-109.

Wilkinson, J., Ueno, K., De Rose, D., Straube, J.F., Fugler, D. 2007. Understanding vapor permeance and condensation in wall assemblies, 11th Canadian Conference on Building Science and Technology Banff, Alberta.

Wilson, A.G. 1965. Condensation in insulated masonry walls in summer, Proceeding of RILEM/CIB Symposium, pp. 2-7.

Økland, Ø. 1998. Convection in highly-insulated building structures, Doctoral Thesis, Department of Building and Construction Engineering, Norwegian University of Science and Technology, Norway.

A.2 Description of stucco cladding

The stucco cladding consisted of two layers of conventional 19 mm cement stucco with no finish layer and had a capillary saturation, $w_{cap,}$ of approximately 232 kg/m^3. The finish acrylic coat was eliminated in order to have a more porous substrate (Figure A.3). The stucco assembly met the requirements of ASTM C 926-98a (Application of Portland Cement-Based Plaster) and ASTM C 1063-99 (Installation of Lathing and Furring to Receive Interior and Exterior Portland Cement-Based Plaster). The stucco layer, consisting of a top scratch coat and a bottom brown coat, was built on a weather resistive barrier (WRB), installed on the exterior sheathing of OSB, over which an expanded galvanized metal lath was installed. The scratch coat of 9 mm consists of 1 part portland cement, 3 parts sand, and 1/2 part lime. The brown coat of 9mm consists of 1 part portland cement, 4 parts sand, 1/2 part lime. In this assembly, the OSB sheathing was the main support and the cladding was not independent from the backwall. The portland cement was Type 10 General Use Portland Cement by Ciment Quebec; dried sand was from Bomix® and Hydrated Lime (Calcium Hydroxide) from Limo Graymont.

The metal lath was held at a distance of 6.35mm from the sheathing (OSB) with spacers in order to allow the scratch coat to penetrate behind the lath and lock into it. The scratch coat was scratched and let dry for a day before application of the brown coat. Scratching ensures better bonding of the brown coat to the scratch coat. The brown coat is finished with a wooden smoothening tool. Figures A.4 and A.5 show the stucco wall during construction.

A moisture uptake test was performed on the stucco specimen to define the capillary moisture uptake of the entire cladding. Knowing the capillary moisture uptake of 232 kg/m^3 for stucco cladding and knowing the total volume of the cladding (1.2 x 2.4 x 0.019m) results in 13 kg of water for the entire stucco cladding to be capillary saturated. For the purpose of the experiment using the stucco cladding, the cladding was subjected to its full capillary moisture uptake. This was achieved using the same method as performed for the brick cladding, with continuously monitoring the mass increase of the specimen during the spraying process.

As the change of mass of the stucco cladding could not be monitored independently from the backwall, small gravimetric samples were also incorporated into the stucco specimen in order to be able to monitor the moisture content of stucco at different heights during the test period. These gravimetric samples were built within a PVC rings which were placed into bigger PVC rings that were fixed into the large-scale specimen (Figure A.6). The construction of the small gravimetric samples was identical to the rest of the wall with the metal lath (6.35 mm away from OSB), the scratch coat and the brown coat. The PVC rings containing the stucco specimen were equipped with two small screws used as handles to easily pull out the sample for the purpose of weighing. The contact surface between the two PVC rings was coated with vacuum grease to ease the process of removing the samples.

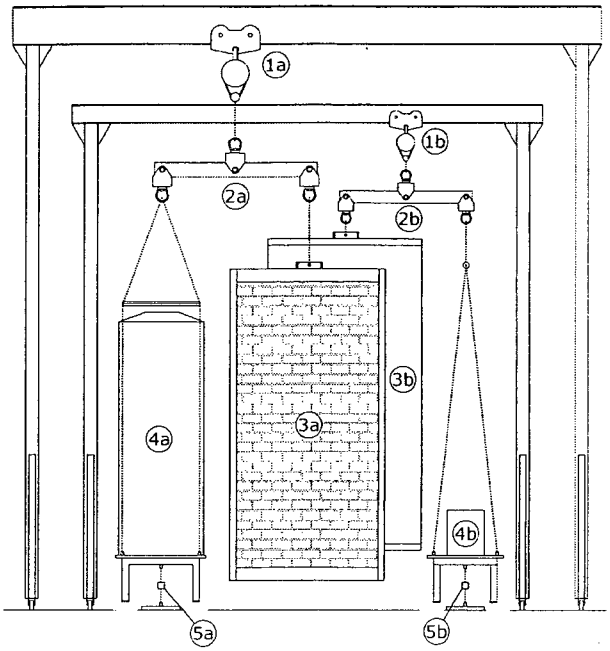

Fig. B. 6 Components and arrangement of the weighing system: 1a – Supporting system, mass capacity of three tons; 1b – Supporting system, mass capacity of one ton; 2a, 2b – Lever arms; 3a – brick cladding or stucco wall; 3b – back wall; 4a – Counter weight, 760 l

Two adjustable cranes were utilized: model Gorbel AG-1-10/15-12 with the capacity of one ton and model Gorbel AG-3-12/15-15 with the capacity of three tons. Two types of trolleys were utilized: Model Coffing CBTP-0100 with mass capacity of one ton and model Coffing CBTP-0300 with mass capacity of three tons. The trolleys allowed horizontal movement of the test specimens along the cranes. The lever arms, constructed of hollow rectangular steel tubes, balanced the specimens in equilibrium, with the specimens being at one end and an object of equal mass being at the other end with equal distances from the central pivot (fulcrum). The center pivot was connected to the crane. Each pivot point consisted of a swivel, bolts and ball bearings. During testing, when the specimen changed mass due to loss or gain of moisture, this setup of the lever arm allowed for easy upwards or downwards movement, minimizing any friction.

Counter weights

The counter weights used for each of the specimen had to have an adaptable mass so that it could be changed with each different specimen to balance it on the leaver arm. By suspending the specimen and its counter weight in equilibrium, any mass change to the specimen could be measured without knowing the overall mass of the specimen.

Water tanks were used as counter weights. A 760 liter (200 gallon) tank was used for the brick cladding and stucco specimen (Figure B.7) and two 20 liter jugs were used for the backwall (Figure B.8). The counter weights were supported on steel tables which were connected to the lever arms using steel chains. The tables were there to protect the load cells in case of improper manipulation.

Appendix J

RH sensor calibration

J.1 Wall 1 (brick, VWC):

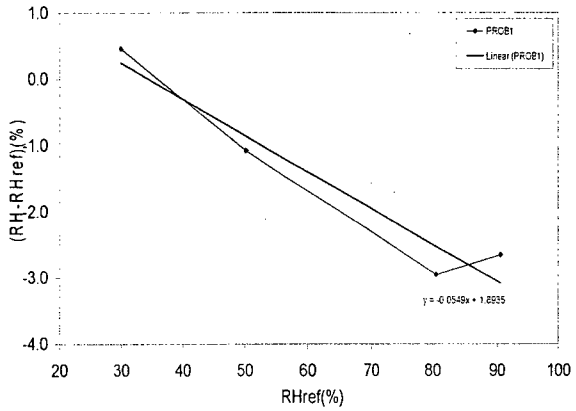

Fig. J. 1 Calibration curve of the outside RH sensor of wall 1

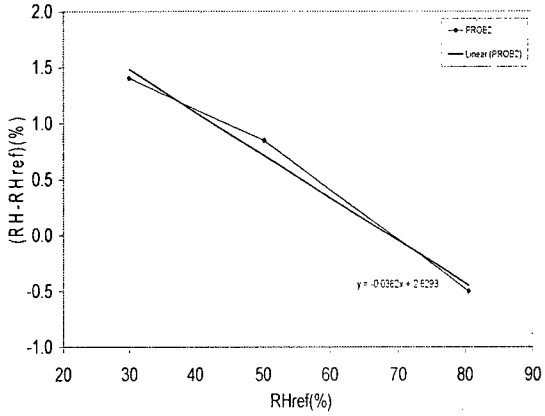

Fig. J. 2 Calibration curve of the inside RH sensor of wall 1

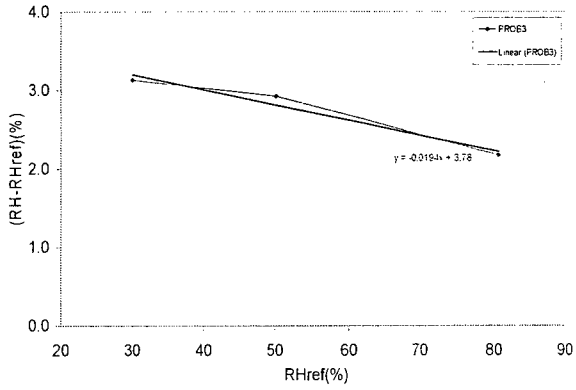

Fig. J. 3 Calibration curve of the insulation cavity RH sensor of wall 1

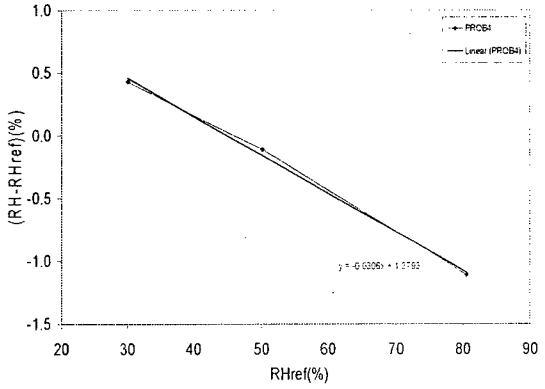

Fig. J. 4 Calibration curve of the air cavity RH sensor of wall 1

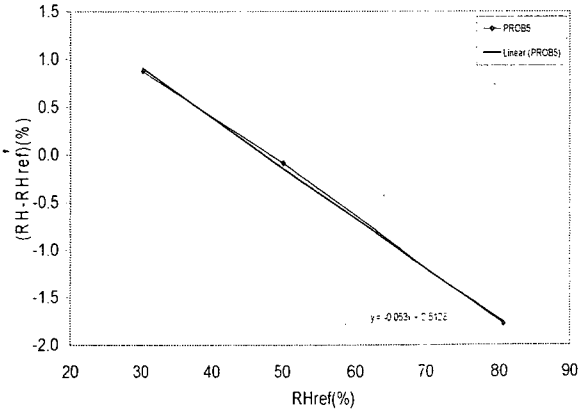

Fig. J. 5 Calibration curve of the laboratory RH sensor of wall 1

J.2 Wall 2 (brick, paint):

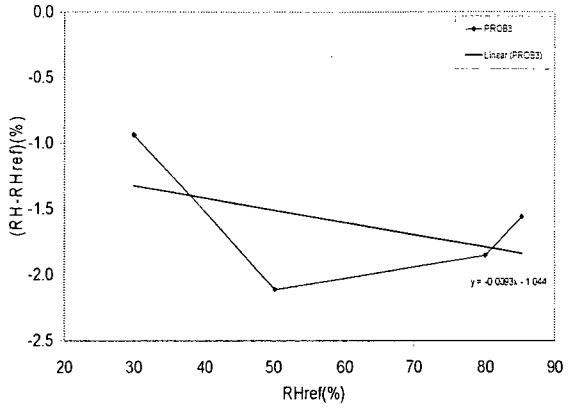

Fig. J. 6 Calibration curve of the outside RH sensor of wall 2

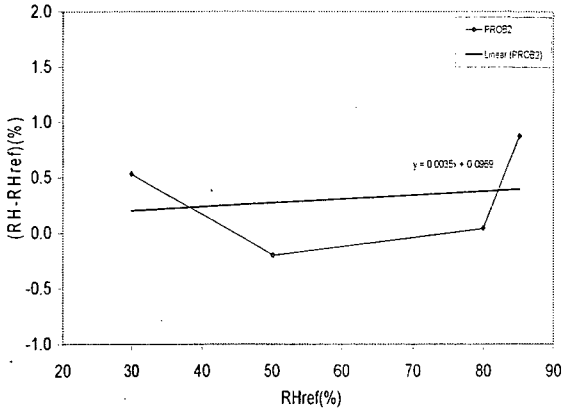

Fig. J. 7 Calibration curve of the inside RH sensor of wall 2

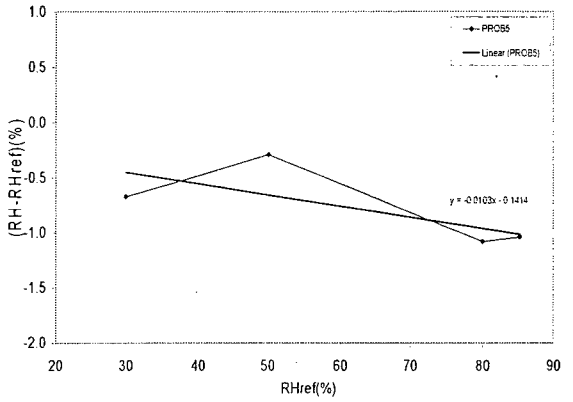

Fig. J. 8 Calibration curve of the insulation cavity RH sensor of wall 2

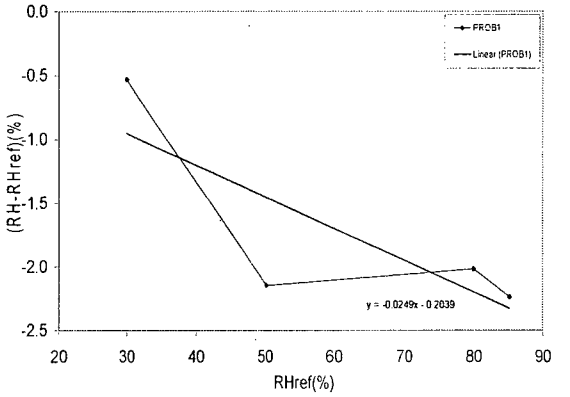

Fig. J. 9 Calibration curve of the air cavity RH sensor of wall 2

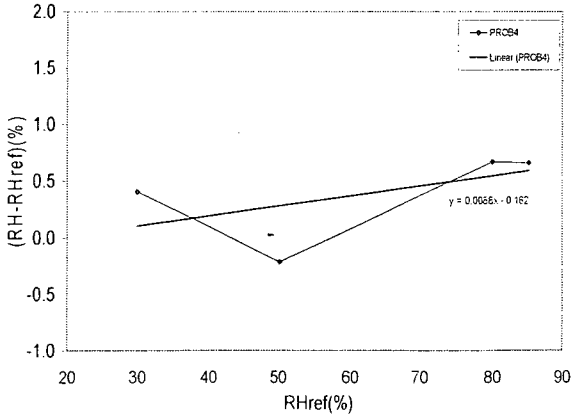

Fig. J. 10 Calibration curve of the laboratory RH sensor of wall 2

J.3 Wall 3 (brick, XPS, VWC):

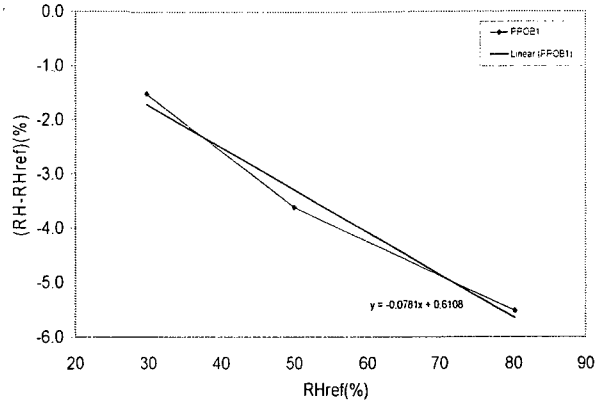

Fig. J. 11 Calibration curve of the outside RH sensor of wall 3

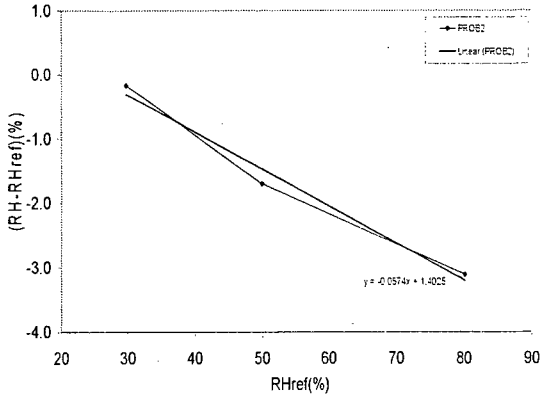

Fig. J. 12 Calibration curve of the inside RH sensor of wall 3

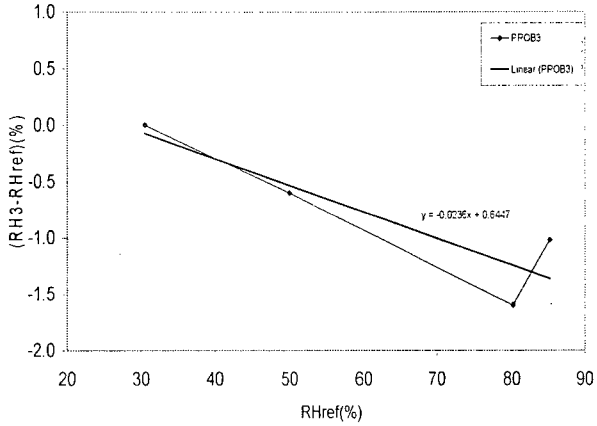

Fig. J. 13 Calibration curve of the insulation cavity RH sensor of wall 3

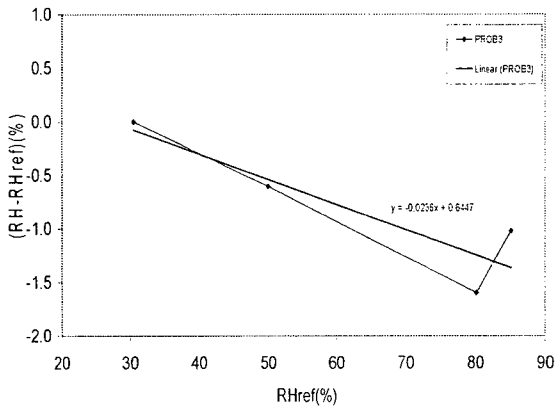

Fig. J. 14 Calibration curve of the air cavity RH sensor of wall 3

J.4 Wall 4 (stucco, VWC):

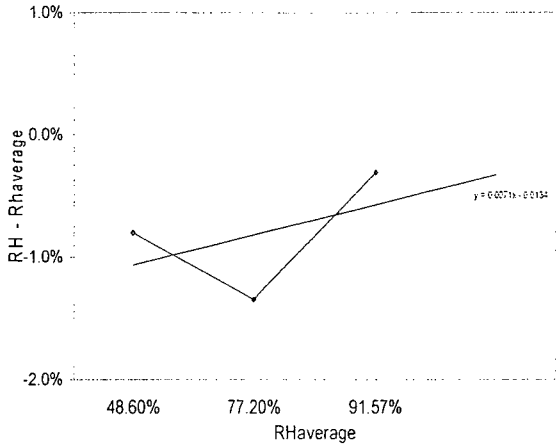

Fig. J. 15 Calibration curve of the outside RH sensor of wall 4

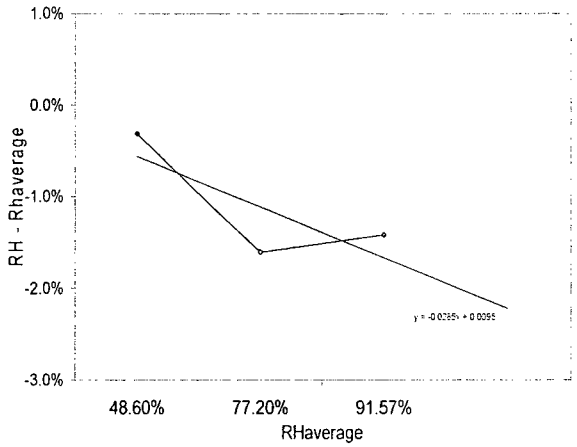

Fig. J. 16 Calibration curve of the inside RH sensor of wall 4

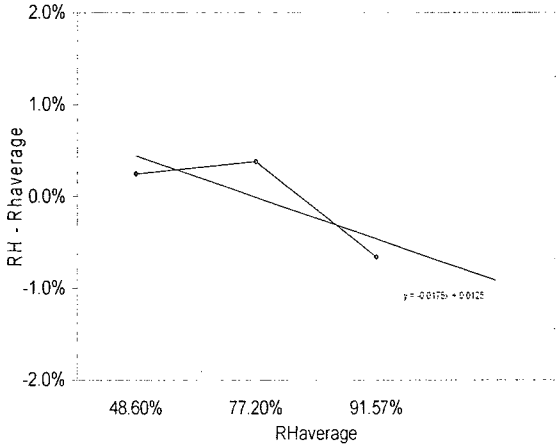

Fig. J. 17 Calibration curve of the insulation cavity RH sensor of wall 4

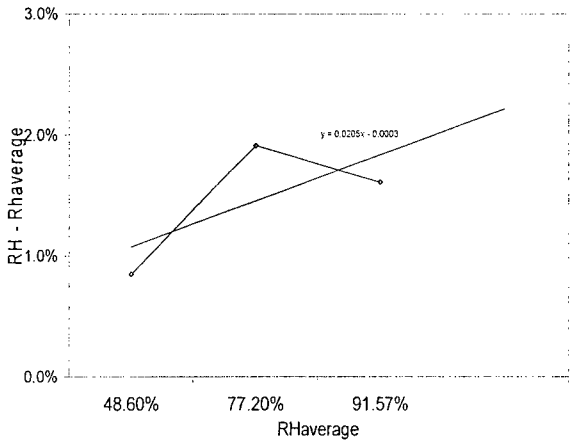

Fig. J. 18 Calibration curve of the laboratory RH sensor of wall 4

J.5 Wall 5 (brick, VWC, vented):

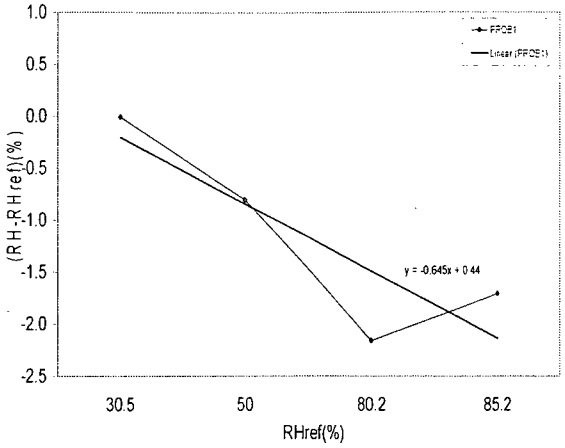

Fig. J. 19 Calibration curve of the outside RH sensor of wall 5

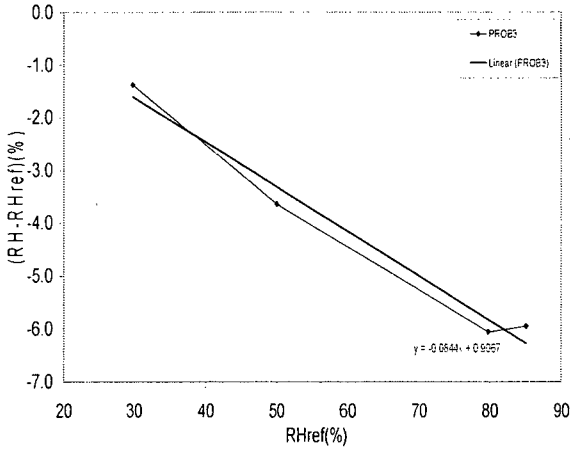

Fig. J. 20 Calibration curve of the inside RH sensor of wall 5

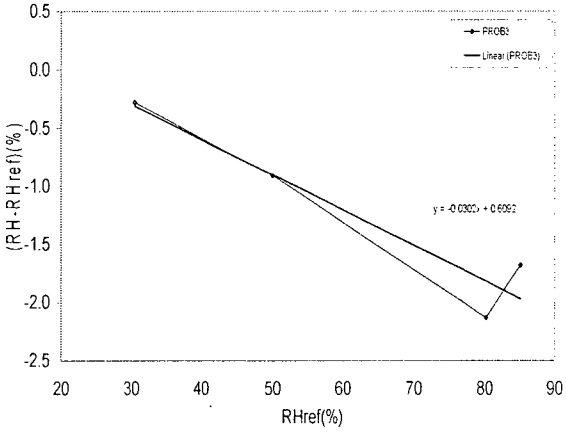

Fig. J. 21 Calibration curve of the insulation cavity RH sensor of wall 5

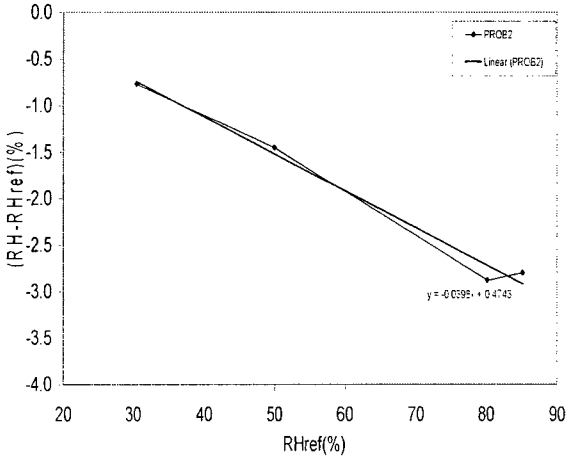

Fig. J. 22 Calibration curve of the air cavity RH sensor of wall 5

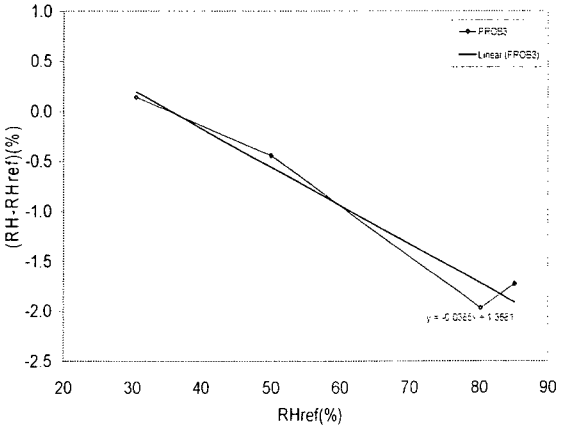

Fig. J. 23 Calibration curve of the laboratory RH sensor of wall 5

Appendix K

Load cell calibration

K.1 Wall 1 (brick, VWC):

Measure mass change of the back wall and brick cladding using the weighing apparatus is corrected using the calibration results of each load cell which was performed before starting the experiment. Figures K.1 and K.2 below show the percentage error of each of the back wall and brick cladding measure using the described calibration procedures.

As we can see, for the weighing system of the brick cladding, the error is approx. %2.5 when the lightest mass was used, and it reached to approx. %6 by the time the wall was loaded with 3.2 kg.

In case of the backwall, the error is quite consistent during the loading period with a sudden increase in the error when a mass of 227 g was utilized.

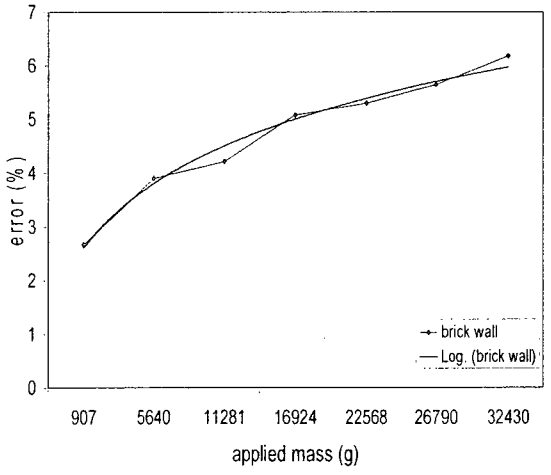

Fig. K. 1 Calibration curve of the brickwall load cell of wall 1

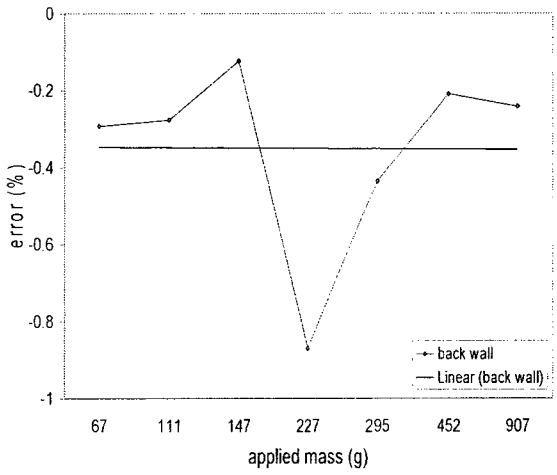

Fig. K. 2 Calibration curve of the backwall load cell of wall 1

K.2 Wall 2 (brick, paint):

Correction of the mass measurements of the back wall and brick cladding using the weighing apparatus is done as was described for the previous wall. Figures K.3 and K.4 below show the percentage error of each of the back wall and brick cladding measure using the described calibration procedures.

As we can see, for the weighing system of the brick cladding, the error is approx. %1.1 when the lightest mass was used, and it reached to approx. %1.8 by the time the wall was loaded with 32 kg.

In case of the back wall, the error was approx. -0.27% using the lightest mass, and it reached a maximum of 0.47% using the heaviest mass of 907 g.

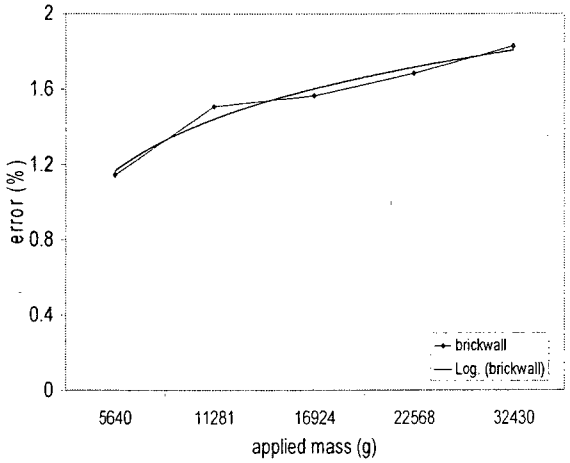

Fig. K. 3 Calibration curve of the brickwall load cell of wall 2

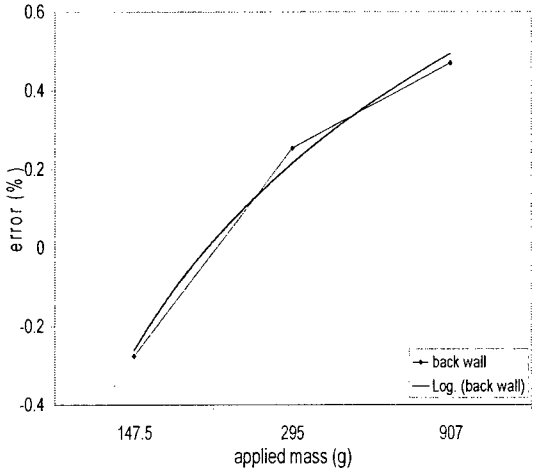

Fig. K. 4 Calibration curve of the backwall load cell of wall 2

K.3 Wall 3 (brick, XPS, VWC):

Correction of the mass measurements of the back wall and brick cladding using the weighing apparatus is done as was described for the previous wall. Figures K.5 and K.6 below show the percentage error of each of the back wall and brick cladding measure using the described calibration procedures.

As we can see, for the weighing system of the brick cladding, the error is approx. % 0.18 when the lightest mass was used, and it reached to approx. %0.65 by the time the wall was loaded with 27 kg.

In case of the back wall, the error was 0.15 % using the lightest mass, and it reached a maximum of 0.61% using the heaviest mass of 591 g.

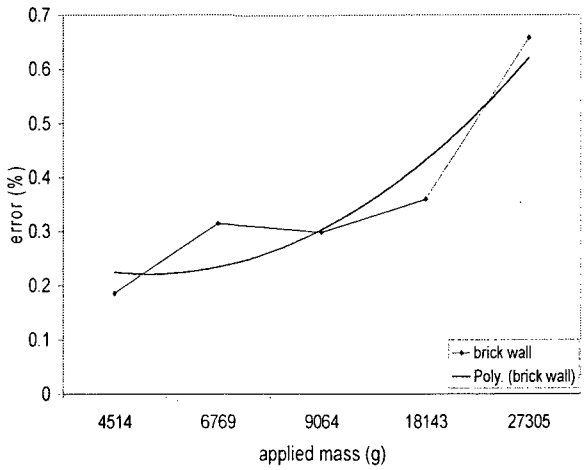

Fig. K. 5 Calibration curve of the brickwall load cell of wall 3

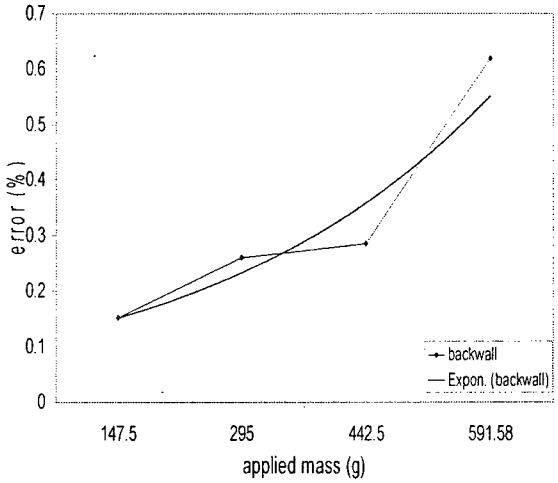

Fig. K. 6 Calibration curve of the backwall load cell of wall 3

K.4 Wall 4 (stucco, VWC):

Correction of the mass measurements of the stucco wall using the weighing apparatus is done as was described for the previous wall. Figure K.7 below shows the percentage error of the wall measured using the described calibration procedures.

As we can see, for the weighing system of the stucco wall, the error is approx. % 0.03 when the lightest mass was used, it increased to %0.8 using a 18 kg mass, and decreased to approx. %0.7 by the time the wall was loaded with 22 kg.

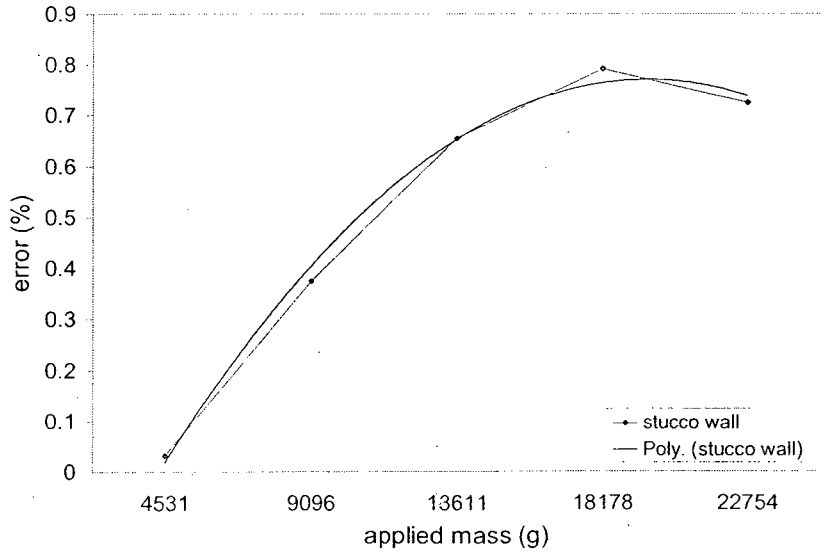

Fig. K. 7 Calibration curve of the load cell of wall 4

K.5 Wall 5 (brick, VWC, vented):

Correction of the mass measurements of the back wall and brick cladding using the weighing apparatus is done as was described for the previous wall. Figures K.8and K.9 below show the percentage error of each of the back wall and brick cladding measure using the described calibration procedures.

As we can see, for the weighing system of the brick cladding, the error is approx. % 1.05 when the lightest mass was used, and it reached to approx. %0.83 by the time the wall was loaded with 27 kg.

In case of the back wall, the error was 0.86 % using the lightest mass, and it reached a maximum of 1.5 % using the heaviest mass of 926 g.

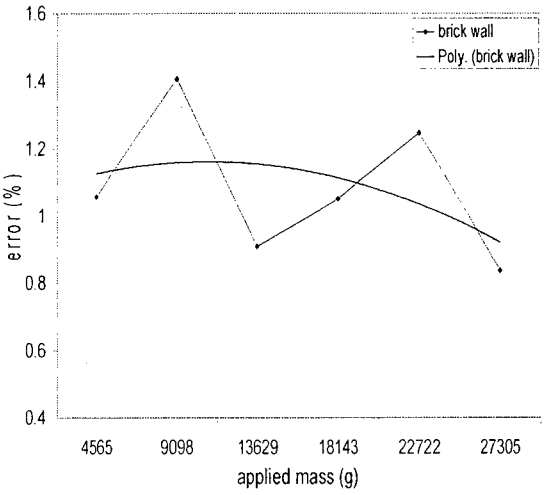

Fig. K. 8 Calibration curve of the brickwall load cell of wall 5

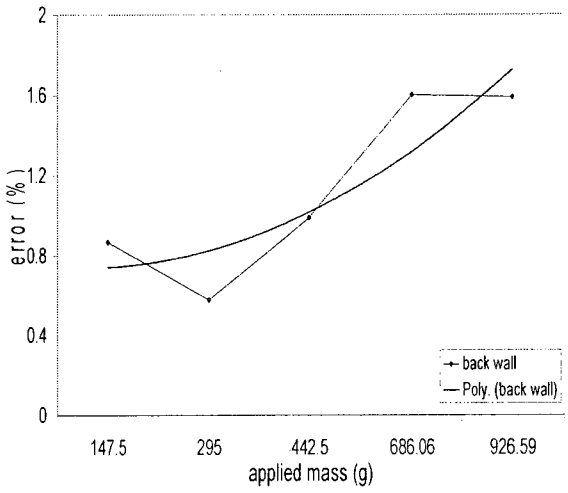

Fig. K. 9 Calibration curve of the backwall load cell of wall 5